BIOGEOCHEMICAL ALTERATION EFFECTS ON U-TH DATING OF PLEISTOCENE CORALS

A THESIS SUBMITTED TO THE GRADUATE DIVISION OF THE UNIVERSITY OF HAWAIʻI AT MĀNOA IN PARTIAL FULFILLMENT OF THE REQUIREMENTS FOR THE DEGREE OF

MASTER OF SCIENCE

IN

GEOLOGY AND GEOPHYSICS

DECEMBER 2018

by

Katherine E Herries

Thesis Committee:

Ken Rubin, Chairperson

Gregory Ravizza

Eric Hellebrand

Keywords: geochemistry, corals, geochronology, uranium series, age dating, sea level rise, paleoclimate, last deglacial, diagenesis, coral alterations

1. ACKNOWLEDGEMENTS

I thank advisor and committee chair Ken Rubin for conceiving and developing this project, and my committee members Gregory Ravizza and Eric Hellebrand for their support and expertise. Their knowledge and guidance has elevated the content and presentation of the research herein.

We thank Denys Vonderhaar, Jasper Konter, Val Finlayson, and JoAnn Stinton for help with laboratory practices. Special thanks to Hawai‘ian Underwater Research Lab, NOAA’s Undersea Research Program, and Schmidt Ocean Institute for their time, expertise, ships, HOVs, and ROVs that allowed us to study this area and collect samples. Part of this research was funded by the Howard E. Stearn’s Fellowship through the University of Hawai‘i’s Department of Earth Science.

Above all, I thank my family and loved ones for the ongoing support through my life, especially in the last two and a half years. Their commitment to me gave me the strength and will to complete this work that I am extremely proud of.

2. ABSTRACT

U-Th geochronology has been used to determine ages of fossilized coral specimens during the late Pleistocene deglaciation. This dating technique allows for a more precise determination of specific relative sea level (RSL) events, such as meltwater pulses. Meltwater Pulse 1a (MWP-1a) has been studied at far-field RSL sites around the globe. This study focuses on a well-preserved fossil coral record from Penguin Bank, a submerged platform off the southwestern coast of Molokaʻi in the Hawaiian Islands. Unpublished Th-U data by Rubin and Fletcher (2012) show that there was a 21±3 mm/yr relative sea level change over the course of the deglaciation at Penguin Bank, off the southwestern coast of Molokaʻi, from 17 to 14.8ka.

This study has provided a more robust determination of RSL and dating fossilized coral reefs at Penguin Bank during one interval of the deglaciation centered around Meltwater Pulse 1a (defined below). The shallow portions of Penguin Bank are currently a thriving mesophotic coral ecosystem with a large coralline algae and deep sea coral population. This study analyzes the effect of these organisms on the geochemistry of fossilized coral specimens. The specimens were observed under an optical microscope and electron microprobe. Three separate textures were found: pristine primary aragonite, secondary aragonite cement, and secondary calcite cement. The abundance of secondary cements increased in areas of alterations. U-Th dates were calculated for specimens with different types of alteration, such as sponge, coralline algae, bioerosion, and discoloration. The compositional difference in pristine sections and altered sections of each coral was measured. Crustose coralline algae, sponges, and bioerosion all have varying effects on precision of calculated ages. Discoloration did not affect the calculated ages in our samples. More data is needed to fully determine the mechanisms causing these changes.

The data collected in this study are in agreement with previously dated corals from Penguin Bank. There is a relationship with sea level change and coral growth and depth, until the onset of MWP-1a, where the corals continue to grow in deeper water instead of keeping up with rising seas. This data will be used in the future to refine the timing of MWP-1a at Penguin Bank and around the globe.

3. List of Figures

4. List of Tables

5. Table of Contents

6. Introduction

U-series geochronology has been used to date fossilized coral reefs. These reefs provide a snapshot of what ocean environments and levels were at the time of their growth. Due to the incorporation of uranium into the calcium carbonate skeleton as well as the half-life, U-Th dating is appropriate for Quaternary and Late Pleistocene geologic and oceanographic events (Edwards et al., 1987). The crux of U-series geochronology relies on the assumption of "pristine" coral skeleton, closed with respect to U and Th, "zero" intial ^{230}Th, and has no visible recrystallization, alterations, or physical disparities. However, "pristine" coral specimens are not widely available due to subaerial exposure, biochemical alterations, and physical/mechanical variations.

In order to accurately date and understand past ocean events, such as rapid sea level fluctuations, the effects and variations due to biogeochemical changes in coral specimens must be understood. In this study, we investigated a suite of corals from a known depth and an assumed age at Penguin Bank, a submerged reef platform off the southwestern coast of the Island of Moloka'i. All specimens grew during the last deglaciation, more specifically, during Meltwater Pulse 1a (~14ka). All specimens have been physically or biochemically altered by the mesophotic ecosystem that is currently thriving at Penguin Bank. This study aims to measure the variations in calculated ages within any given altered coral specimen and provide further implications for using coral specimens to define specific ocean/sea level events.

The following introduction presents an overview of sea level change since the Last Glacial Maximum, focusing on Meltwater Pulse 1a (MWP-1a). This section summarizes previous work for MWP-1a around the globe and Penguin Bank. Second, it further provides an overview of the use of U-series geochronology for dating fossilized coral specimens, outlining specifics for

understanding the variation seen in the coral specimens. Next, it introduces the study area in more detail. Finally, it provides an overview of the thesis work that will be presented.

6.1 Sea Level and Meltwater Pulse 1a

During the last deglaciation, sea level did not rise at a constant rate. The rapid retreat of the continental ice sheets caused drastic increases of ocean volume, called "meltwater pulses." Evidence of meltwater pulses have been documented around the globe using fossilized coral reefs. These reefs provide a snapshot of what ocean environments (acidity, temperature, etc) and sea levels were at the time of their growth. U-series geochronology is perfectly suited for dating coral specimens from the early Quaternary and late Pleistocene (Edwards et al., 1987).

The Last Glacial Maximum (LGM) occurred from 26-20ka before present (BP), when vast continental ice sheets covered the Earth (Clark et al., 2009; Peltier, 2002). The ice sheets started retreating ~20ka, causing changes in sea level around the globe. From the LGM to present, there has been an eustatic, or uniformly global, increase in sea level of ~120m (Fleming et al., 1998; Peltier, 2005). The average rate of rise was about 12m/ka from about 16.5ka to 8.2ka BP (Lambeck et al., 2014). The majority of the changes in ocean volume came from the largest of the ice sheets the Laurentide and West Antarctic ice sheets (Bentley et al., 2010; Golledge et al., 2014; Gomez et al., 2015; Liu et al., 2016; Tarasov and Peltier, 2006).

Periods of gradual sea level rise were punctuated by periods of greater rates, or "meltwater pulses." The speed and magnitude of these pulses suggest the collapse of some portions of ice sheets as opposed to accelerated deglaciation of any ice sheet. The collapse of the ice sheets and opening, and subsequent draining, of large glacial lakes, created a release of glacial meltwater into the ocean (Blanchon and Shaw, 1995; Clark et al., 1996; Fairbanks, 1989).

The most well-studied of these pulses Meltwater Pulse 1a (MWP-1a) (Clark et al., 1996; Deschamps et al., 2012; Gregoire et al. , 2012). MWP-1a occurred ~14ka BP with an average rate of sea level rise of ~45mm/yr (Clark et al., 1996). This pulse of very rapid sea level rise was first documented in a core of a fossilized reef in Barbados, and since has been recorded in reefs in Tahiti, Hawai‘i, the Sunda Shelf, the Hunon Peninsula, and the Great Barrier Reef (Bard, 1990; Deschamps et al., 2012; Gregoire et al., 2012; Hanebuth et al., 2000; Sanborn et al., 2017; Webster et al., 2004, Rubin and Fletcher, 2012). However, the observational uncertainties for this specific pulse remain large, including differences in the timing of this event as recorded at different localities.

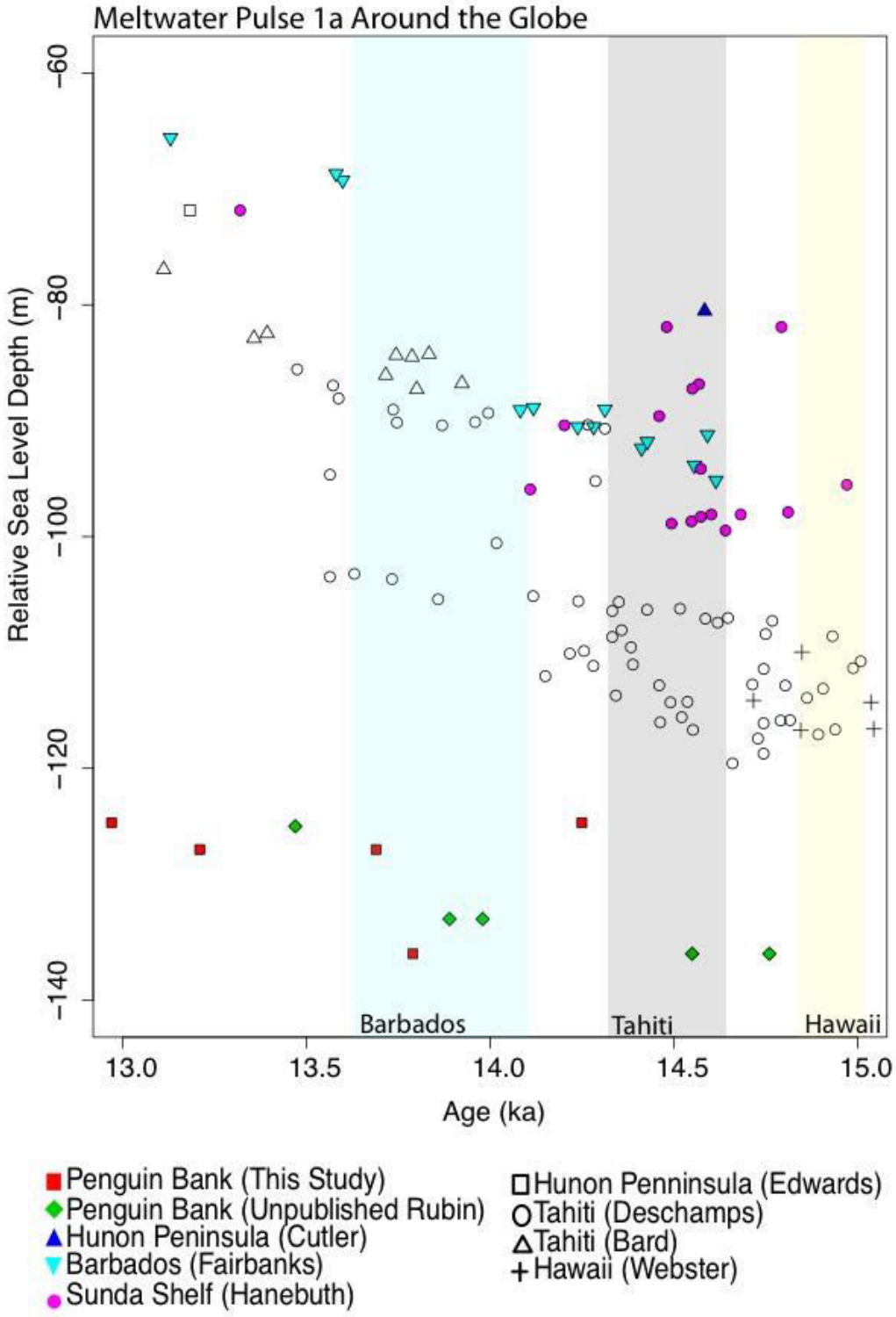
Meltwater Pulse 1a Around the Globe
Relative Sea Level Depth (m)
−60
−80
−100
−120
−140
Barbados
Tahiti
Hawaii
13.0
13.5
14.0
14.5
15.0
Age (ka)
Penguin Bank (This Study)
Penguin Bank (Unpublished Rubin)
Hunon Peninsula (Cutler)
Barbados (Fairbanks)
Sunda Shelf (Hanebuth)
Hunon Penninsula (Edwards)
Tahiti (Deschamps)
Tahiti (Bard)
Hawaii (Webster)

Figure 1. Figure edited from Sanborn et al., 2017 with new Penguin Bank data (red squares, this study and green diamond, unpublished Rubin). Plotted are global sea-level records, based on coral ages and reconstructed paleo-depth/elevation. including Tahiti (unfilled triangles, Bard et al., 2010 circles, Deschamps et al., 2012), Barbados (teal upside down triangle, Fairbanks et al., 2005 and Peltier & Fairbanks, 2006), Hunon Peninsula, Paupa New Guinea (blue triangle, Edwards et al., 1993; unfilled square, Cutler et al., 2003), and Sunda Shelf (pink circles, Hanebuth et al., 2000). The vertical bands indicate timing of MWP-1a based on the Tahiti (grey band, 14.65-14.3ka; Deschamps et al., 2012, Camoin et al., 2012), Barbados (teal band, 14.08-13.61ka, Fairbanks, 1989), and Hawai‘i (yellow band, 15.2-14.7ka, Webster et al., 2004). Error bars are not shown in this figure.

The Tahiti record shows between a 14-18 m rise in sea level in 350 years from 14.65-14.3ka (Camoin et al., 2012; Deschamps et al., 2012). The Barbados record shows a similar magnitude but for 500 years and about 300 years later (14.08-13.61ka) than Tahiti (Abdul et al., 2016; Bard et al., 1990; Stanford et al., 2006). Drowned reef structures off the island of Hawai‘i date about 15.2-14.7ka with about 35m in <500years at a rate of 50-40mm/yr. (Sanborn et al., 2017; Webster et al., 2004). Unpublished U-Th data by Rubin and Fletcher (2012) show that there was a 0.021±0.003 m/yr relative sea level change at Penguin Bank, a submerged reef platform off the southwestern coast of Moloka‘i, from 17 to 14.8ka (Rubin and Fletcher, 2012).

For reconstruction of sea level using coral reefs, one must reconstruct paleodepth of the present day reef. Tahiti, Barbados, and the island of Hawai‘i have all experienced a tectonic shift during the last 20ka. These tectonic movements have to be corrected out in order for relative sea level rise to be established. Tahiti’s record is corrected for a subsidence of 0.25 mm yr^{-1} (Deschamps et al., 2012; Camoin et al., 2012). A onshore exposure of reef in Barbados indicates that the south coast has been uplifted at a rate of ~ 34 cm kyr^{-1} (Fairbanks, 1989). Published data for the island of Hawai‘i show estimates of subsidence at about 2.5 mm yr^{-1} (Webster et al., 2004). The difference in all these tectonic regimes and the ability to correct the subsidence or uplift out of the current depth plays a significant role in the differences seen in each area.

There is little recorded data for the tectonic motion of Moloka‘i. Watts and ten Brink (1989) showed that Molokai is positioned right on the hinge point between the subsidence of the island of Hawaii and the uplift of the outer islands due to lithosphere flexure (Oahu uplift: 0.02 to 0.05 mm yr^{-1}; Grigg and Jones, 1997; Muhs and Szabo, 1994)). However, newer published data shows uplift (Rubin et al., 2000) or subsidence for Lanai (Webster et al., 2006). Therefore, the bounds on tectonic motion for Penguin Bank would be within 3m during the last 15ka, which is essentially stable for the purposes of reconstruction.

Due to the placement of glaciers, rates at which they melt, and other environmental factors, sea level did not change uniformly (Clark et al. , 2002). Spatial variation in MWP-1a’s amplitude can be expected because of the planet’s elastic and gravitational response to rapid unloading of ice in either or both of the two hemispheres (Lambeck et al., 2014; Whitehouse, 2009). The rebound of the lithosphere from glacial unloading creates a smaller relative sea-level change in areas closer to the glacier. Glacial far-field sites, such as fossil coral reefs far from glaciers in tropical regions, allow for measurement of relative sea level without factoring in glacio-isostatic rebound (Bassett et al., 2007). Hawai‘i is one such far-field site. The average RSL anomalies between the LGM and present are very small (Fleming et al., 1998; Lambeck et al., 2014; Peltier, 2002). Any sea level change seen in Hawai‘i was not substantially influenced by the isostatic rebound of melting continental glaciers.

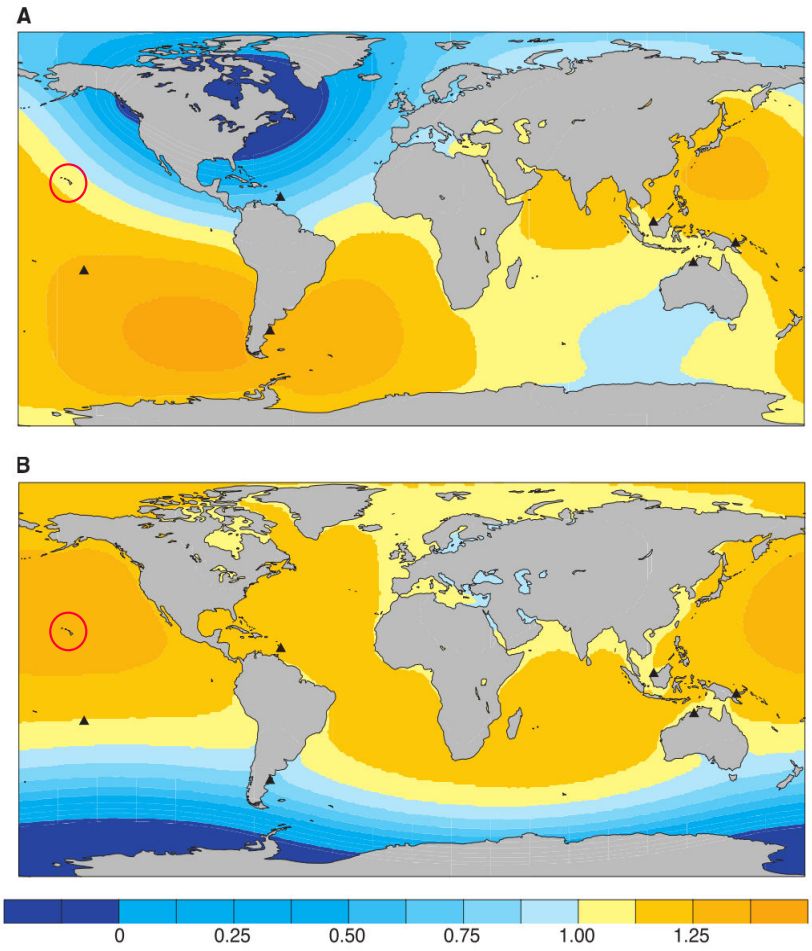

Figure 2. Normalized sea-level change plot edited from Clark et al., 2002 to show placement of the Hawaiian Islands. Figure shows the melting and subsequent sea level change from (a) the southern 1/3 of Laurentide Ice Sheet and (b) Western Antarctica. Edited from Clark et al., 2012

The glacial source for MWP-1a is integral to understanding the distribution of sea level change. The Laurentide Ice Sheet is mostly noted as the source for MWP-1a because of its size, with evidence limited to deep-sea cores from the Gulf of Mexico and the Bermuda Rise (Carlson et al., 2012; P U Clark et al., 2002). However, there was an onset of retreat of the West Antarctica Ice sheet about 14.5ka, which is concurrent with the production of MWP-1a (Clark et al., 2009; Weber et al., 2014). The data known today from Barbados, Tahiti, Sunda Shelf point towards a mixed meltwater signal from both the Laurentide and West Antarctic Ice Sheets

(Bentley et al., 2010; Golledge et al., 2014; Gomez et al., 2015; Liu et al., 2016; Tarasov and Peltier, 2006).

6.2 Coral Reefs and U-series Geochronology

Studies of coral reef records from the last deglaciation are important in order to constrain the timing and magnitude of rapid sea-level rise and in understanding the reef response to dramatic environmental perturbations (Blanchon and Shaw, 1995). As the sea levels rise, Neumann and Macintyre (1985) suggest that there are three distinct ways coral reefs react: (i) "keep-up", where the reef grows upward with the rising sea levels, (ii) "catch-up" where the reef initially grows in deeper portion as sea level rises, but then quickly grows back up to sea level, possibly due to a decrease in rate of sea level rise, and (iii) "give-up" where the reef is unable to adapt to rising sea levels and there is a cessation in reef growth (Hibbert et al., 2016). The maximum vertical accretion rate for coral reefs in the Hawai'ian the geologic record is 10 mm/yr, though this can vary from site to site (R. W. Grigg, 1998; Webster et al., 2004). Though the rate of sea level change at Penguin Bank is recorded at about 21mm/yr, the reef does not show any prominent cessation of growth (K. Rubin, personal communication; Rubin and Fletcher, 2012). The shallow reef forming corals continuously grow throughout the known MWP-1a depth of 140-120mbsl.

U-series geochemistry has been used to determine age/sea level relationships for fossilized coral reefs for many years. Corals incorporate uranium into their skeleton during growth (Hibbert et al., 2016; Lazar et al., 2004). Unlike other trace elements that corals gain as they grow, the mode of U incorporation is still debated. The most abundant U species in seawater

are uranyl carbonate ions, $UO_2(CO_3)_3^{4-}$ and $UO_2(CO_3)_2^{2-}$. The whole unit could be incorporated into aragonite, usually into the carbonate section, essentially intact (Lazar et al., 2004). Uranium (we look specifically at two isotopes: ^{238}U and ^{234}U) is naturally abundant in seawater. As uranium is incorporated into the coral skeleton, the ratio of $^{234}U/^{238}U$ is equal to the $^{234}U/^{238}U$ of the open ocean. The fundamental premise of U-Th dating is that corals incorporate substantial seawater uranium and negligible thorium into their aragonite skeletons during growth, and remain subsequently closed to uranium and thorium loss or gain (Edwards et al. 1987; Thompson et al., 2003) . After the coral dies, the ^{238}U decays to ^{234}U which decays to ^{230Th} which then further decays. The half-lives of each isotope, respectively, are $4.468x10^9$ yrs, $2.455x10^5$ yrs and $7.584x10^4$ yrs. U-series is perfectly poised to date geologic events from the Last Pleistocene (Edwards et al., 1987).

U-Th geochronology relies on the crux of using pristine primary aragonite skeleton for chemistry and analysis. For a reliable age, the skeleton must not have undergone any sort of open-system behavior allowing for movement of U and Th, especially if sample has undergone any sort of diagenesis or chemical alteration. Usually these alterations are determined visually with hand sample and microscope (e.g., Rubin et al., 2000). With the small amount of fossilized coral specimens dating back into the Pleistocene that have not either been subaerially exposed or biogeochemically altered by other mesophotic organisms, pristine skeletons are difficult to ascertain. The changes due to diagenesis and calcite recrystallization due to meteoric water exposure or freshwater infiltration have been extensively documented (Allison, 1996; Enmar et al., 2000; Lazar et al., 2004; Sayani et al., 2011). Potential U-Th mobility, and associated change in calculated dates, due to alteration from mesophotic organisms, such as sponges, crustose coralline algae, and bioeroding organisms have not been studied in depth.

There are methods to use that discuss “open-system” behavior where corals are subject to continuous or episodic addition or subtraction of U-Th (e.g., Scholz & Mangini, 2007; Thompson et al. , 2003). These studies attempt to understand the mechanics of radioactive and geochemical parameters within the coral specimens themselves which could lead to variations in concentrations and activities. There is no “one size fits all” open system model to interpret the data and the mechanisms are still highly contested (Hibbert et al., 2016). Though we will discuss possible open system behaviors for our data, we assume closed-system behavior for our interpretations.

6.3 Geologic Setting

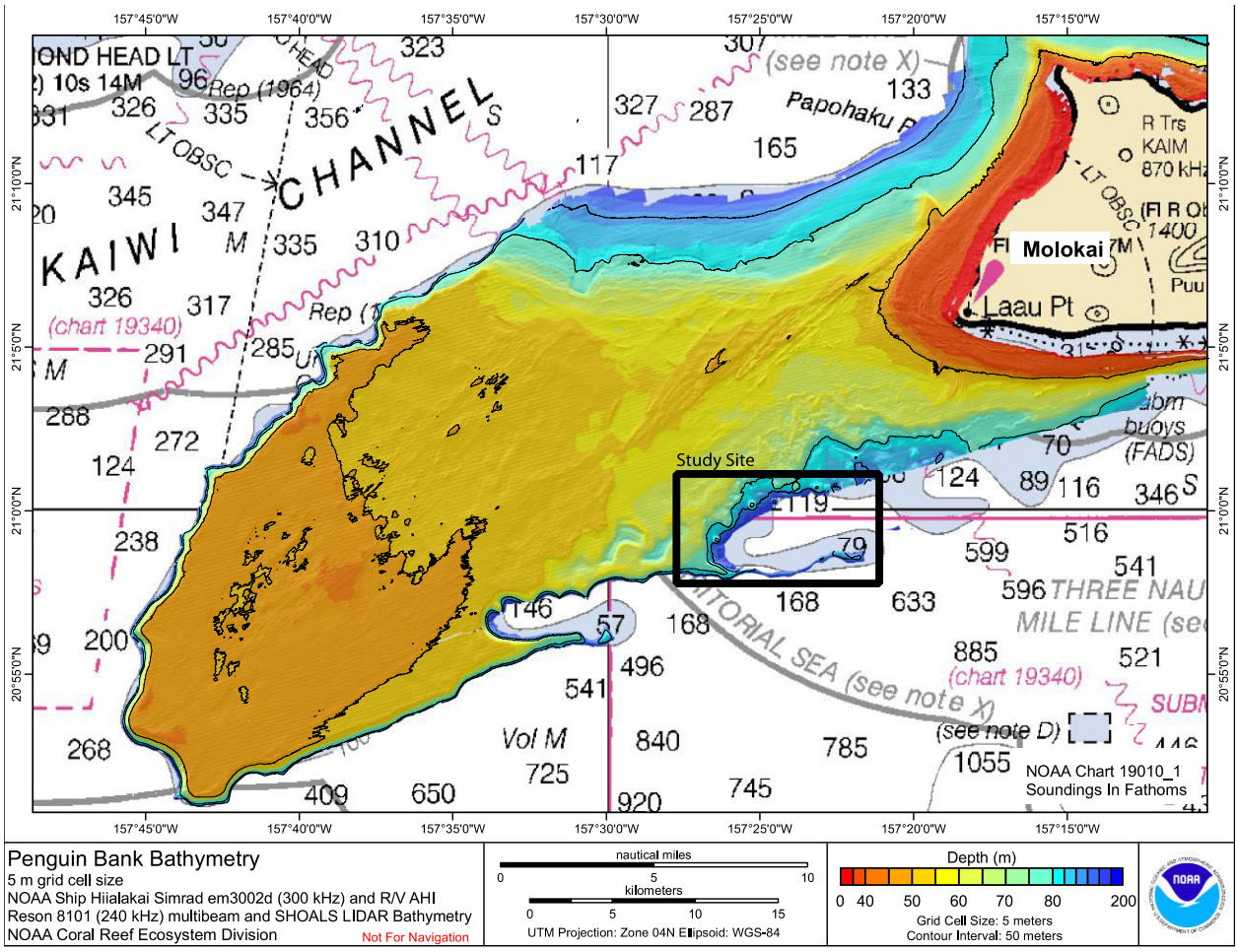

Figure 3. Bathymetric map of Penguin Bank edited from collaboration between NOAA and University of Hawai‘i at Mānoa School of Ocean and Earthl Science and Technology. The black box shows the study area for this thesis work, and all previous work done for this study.

Penguin Bank is a submerged platform off the southwestern coast of the island of Moloka‘i in the Main Hawai‘ian Islands chain. Once a part of the large Maui Nui island complex, Penguin Bank is considered to be either an offshore extension of the West Moloka‘i rift zone or a separate submerged shield volcano. As discussed earlier, as the islands move away from the hotspot, they move from an area of subsidence to an area of uplift (Watts and ten Brink, 1989). The island of Hawai‘i and Maui are currently subsiding, whereas Oahu is currently

uplifting (Fletcher et al., 2008; Muhs et al. , 2003). Moloka‘i is thought to be on the tilt-axis of these two regimes, making it relatively stable.

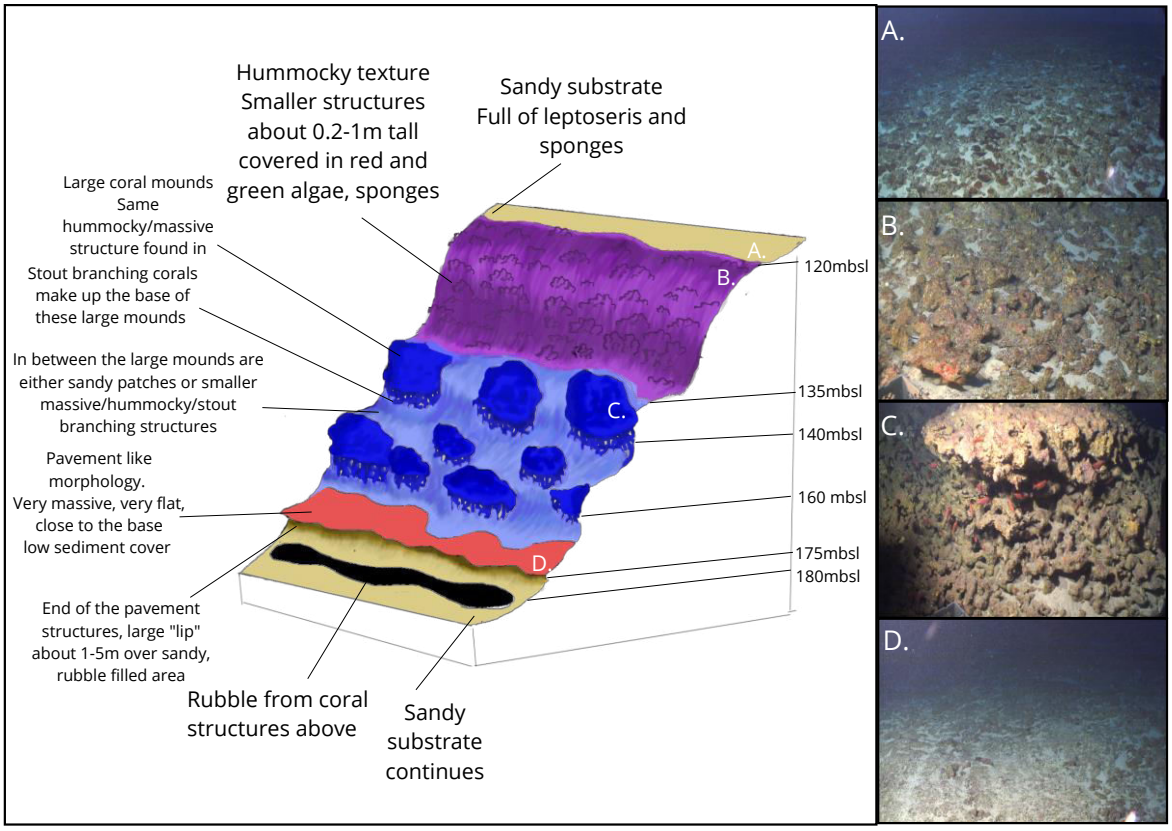

Figure 4. Slope Schematic for Penguin Bank shows the change in coral morphology and mesophotic organisms. This schematic is based upon of hours of submersible dive footage taken over 2007-2017. The colors indicate changes in slope as well as morphology. From top to bottom: Tan – sandy substrate full of *Leptoseris* and spognes; Purple – hummocky texture, smaller structures about 0.2m tall, covered in red and green algae, sponges and *Leptoseris* as depth decreases; Blue – Large coral mounds made up of stout branching corals, some hummocky/massive structures found in shallower depth, but consolidated into 5-20m tall structures separated by about 10m; Light Blue – in between large mounds is either sandy patches or massive/hummocky/stout branching structures; Red – pavement-like structure, very massive, very flat, close to base, low sediment cover, creates an overhang at bottom; black – rubble from coral structures above; Sandy substrate with no mesophotic covering from 180m and deeper. Not to scale.

The whole platform of Penguin Bank itself is about 57-2000m water depth, with a large step-like feature at 500m and sediment at the top. From around 90-300m, a reef (reef-crest) formed on top of a carbonate platform and up along the steep sides of the bank. The deglacial reef is characterized by the main reef building corals endemic to northern Pacific, such as

Porites, *Montipora*, and *Pocilopora*; however, *Porites compressa* seems to be the dominant species during the last deglaciation. This is likely due to the high wave stresses that are generally consistent with southern and Kona swells (Fletcher et al., 2008). The morphology of the corals ranges from massive to fingering. At present, the reef hosts a diverse community of mesophotic life, from fish and sharks to algae and deep sea coral such as *Leptosiris*. There is now limited wave action, strong light penetration to a water depth of about 200m, and a non-existent to limited upslope watershed.

6.4 Objectives

The meltwater signature at Penguin Bank has been studied for the past 10+ years (Rubin and Fletcher, 2012, 2014). To understand the variations in calculated ages due to biogeochemical alterations, this study focuses on specimens specifically from the MWP-1a depth at Penguin Bank. We utilize ages of coral specimens at specific depths based on previously dated corals by K.H. Rubin (2012, 2014). By comparing altered sections and pristine sections of different coral specimens, we hope to qualitatively and quantitatively assess the impact of this type of submarine alteration on calculated ages and potentially contribute to a greater understanding of MWP-1a at Penguin Bank and around the globe.

7. Methods

7.1 Field Methods

7.1.1 Sample Collection

The main study sites at Penguin Bank are located about 13km off the southern shore of the island of Moloka'i, in an area called "the Fingers." Over 140 coral specimens have been collected here between 2007 and 2014. The specimens are a mixture of *Porites, Montipora, Acropora*, and other reef forming corals. The samples in this study are all *Porites compressa*. These samples were collected in situ using the Hawaiian Underwater Research Laboratory (HURL) Human Operated Vehicles (HOV) Pisces IV and V (P4 and P5). The use of manned submersible allows for the distinguishing of reef from debris as well as the exact position and morphology of each specimen.

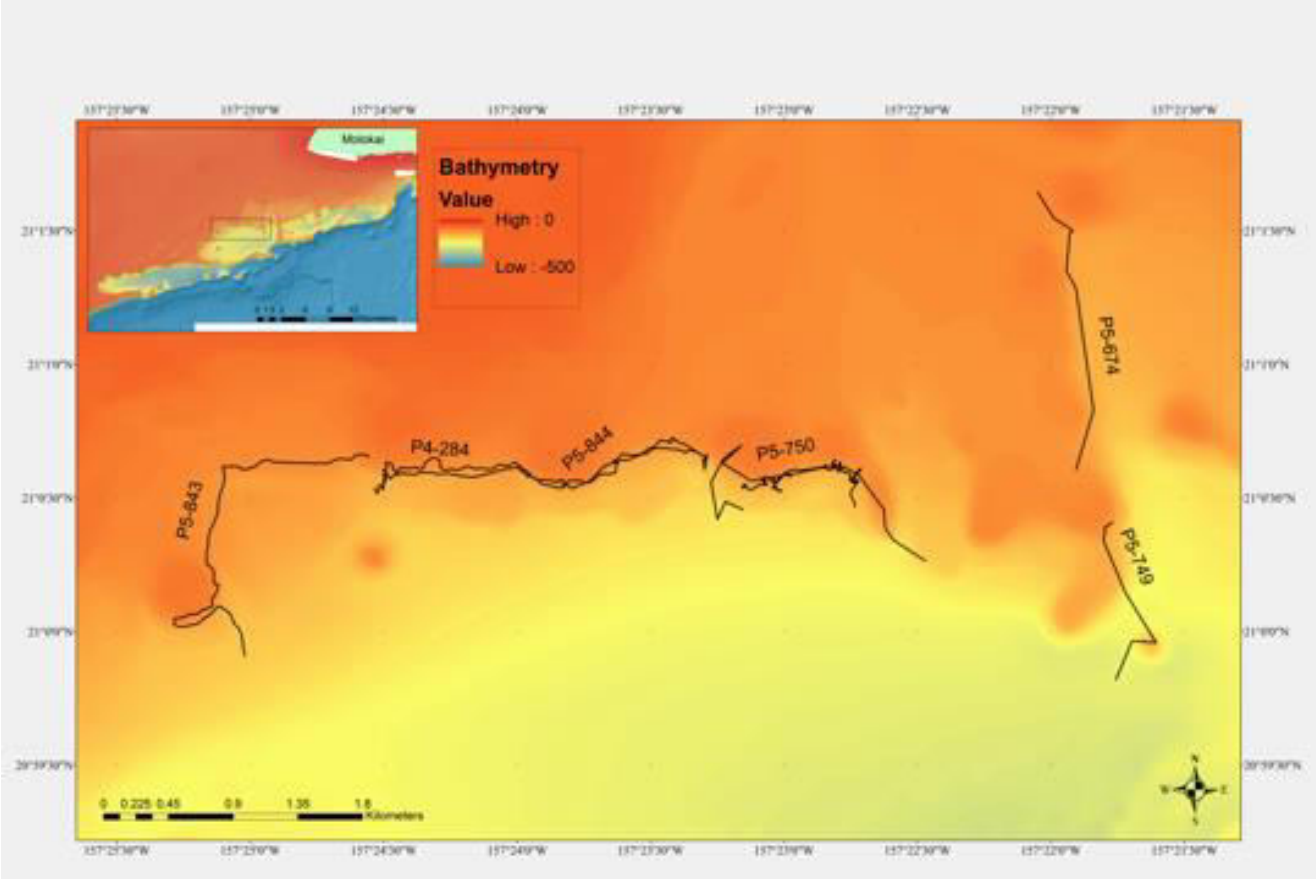

Figure 5. Map of study area at Penguin Bank. Black lines are submersible dive tracks, where samples were collected.

This study uses 10 coral specimens (Table 1) from dives P4-284, P5-749, P5-750, P5-841, P5-843, P5-844, which were completed aboard the University of Hawai‘i R/V Kaimikai-O-Kanaloa (KOK) with HOVs the Pisces IV and V (P4 and P5, respectively) by Dr. Ken Rubin and HURL. The depth, latitude, and longitude of each specimen was determined by the ultra-short baseline system (USBL) and global positioning system (GPS) of the submersibles and the ship. Each sample falls within the previously measured depth range of MWP-1a in this area (Rubin and Fletcher, 2012).

Specimen	*IGSN*	*Latitude*	*Long*	*Depth*	*Genus*	*Morphology*	*Collected By*	*Date Collected*
P4-284-13	KHR30026U	21.0093	-157.39870	-150	Porites	Stout branch	Rubin/UH KOK/Pisces IV	Nov. 2014
P5-749-08	KHR000121	21.0065	-157.36332	-136	Porites	Massive	Rubin/UH KOK/Pisces V	Oct. 2010
P5-750-07	KHR00012D	21.00762	-157.37708	-133	Porites	Massive	Rubin/UH KOK/Pisces V	Oct. 2010
P5-750-11	KHR000131	21.01022	-157.37873	-150	Porites	Stout branch	Rubin/UH KOK/Pisces V	Oct. 2010
P5-841-07	KHR30023O	21.0102	-157.3800	-143.8	Porites	Massive	Rubin/UH KOK/Pisces V	Nov. 2014
P5-841-11	KHR30023S	21.0107	-157.3802	-127	Porites	Massive	Rubin/UH KOK/Pisces V	Nov. 2014
P5-841-17	KHR20023Y	21.0094	-157.3847	-126.7	Porites	Massive	Rubin/UH KOK/Pisces V	Nov. 2014
P5-843-15	KHR30025L	21.0108	-157.4098	-127	Porites	Massive	Rubin/UH KOK/Pisces V	Nov. 2014
P5-844-17	KHR30026D	21.0094	-157.3971	-124.7	Porites	Massive	Rubin/UH KOK/Pisces V	Nov. 2014

Table 1. Table of specimens. “Specimen” is the identifier given to each sample for organization and labeling aboard ship and lab procedures. “P*-###-##” stands for which Pices HOV used – number of dive – number of specimen collected. IGSN (International Geologic Sample Number) correlates to online specimen specifications which will be released. Latitude and Longitude of each sample collected in decimal degrees. The depth is in meters below sea level (msbl) and correlates to the depth the specimen was collected at. All samples can be defined as Porites sp. The physical morphology of specimens range from massive to stout branching, which are common Porites morphologies. All Samples were collected during either a 2010 or a 2014 expedition by Ken Rubin aboard the University of Hawai‘i’s R/V Kaimikai-O-Kanaloa (KOK) with Hawai‘ian Underwater Research Lab’s submersibles Pices IV and V.

After collection with the ROV, the specimens were brought onto the ship. When the specimens were first brought aboard, they were covered in algae, sponges, and other corals. This overgrowth was removed by abrasive scrubbing. Underneath the live organism covering, there commonly was a hard sediment layer. Unless there was a broken face from which coral is visible, the specimens were sawed in half. The number, size, depth, latitude, longitude, physical description, and any other comments were recorded.

7.1.2 Hand Sample Screening

Most specimens have undergone either minor or more extensive biogeochemical alterations through its life and post-mortem. These alterations can affect the U-Th age of a coral specimen. For this reason, we have examined a range of post-mortem alterations. 1) pristine specimens that have none of the aforementioned biogeochemical disturbances; 2) specimens overgrown by crustose coralline algae; 3) specimens overgrown by sponges; 4) specimens that have undergone bioerosion; 5) specimens with staining and discoloration. These five categories can be seen in many of the specimens collected from Penguin Bank.

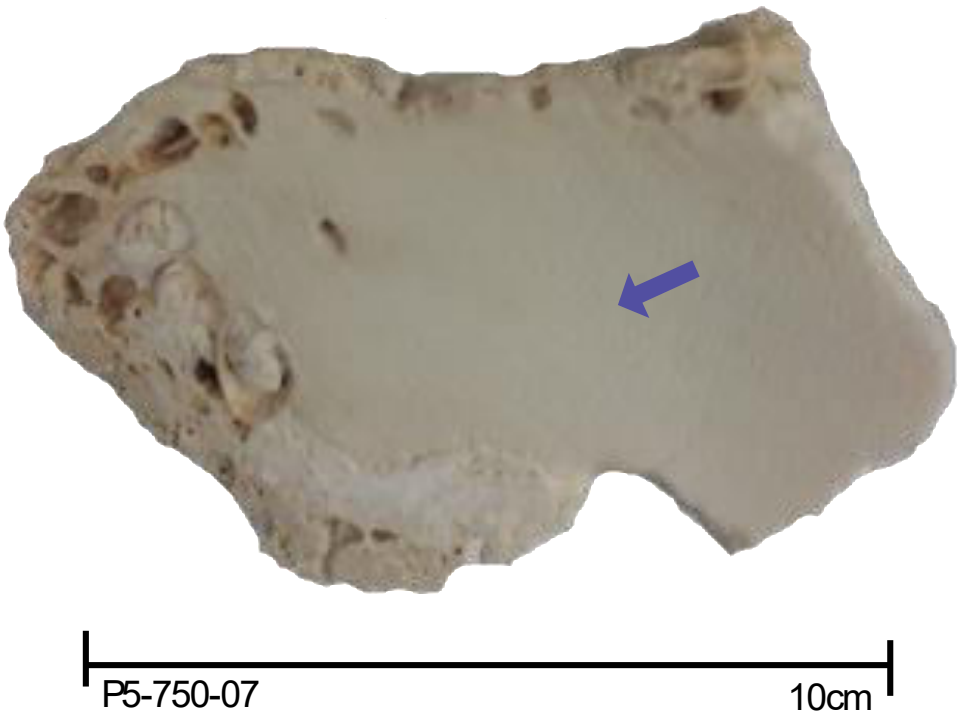

Figure 6. P5-750-07 is category 1 – Pristine - specimen. The blue arrow points out the pristine part of the sample. The coral skeleton is visually unaltered, with complete structure, no detrital material, or pores filled. There is hard sediment covering on the left, but that was avoided when sampling as well as almost completely unavoidable in all specimens. All other pristine sections were compared to this specimen.

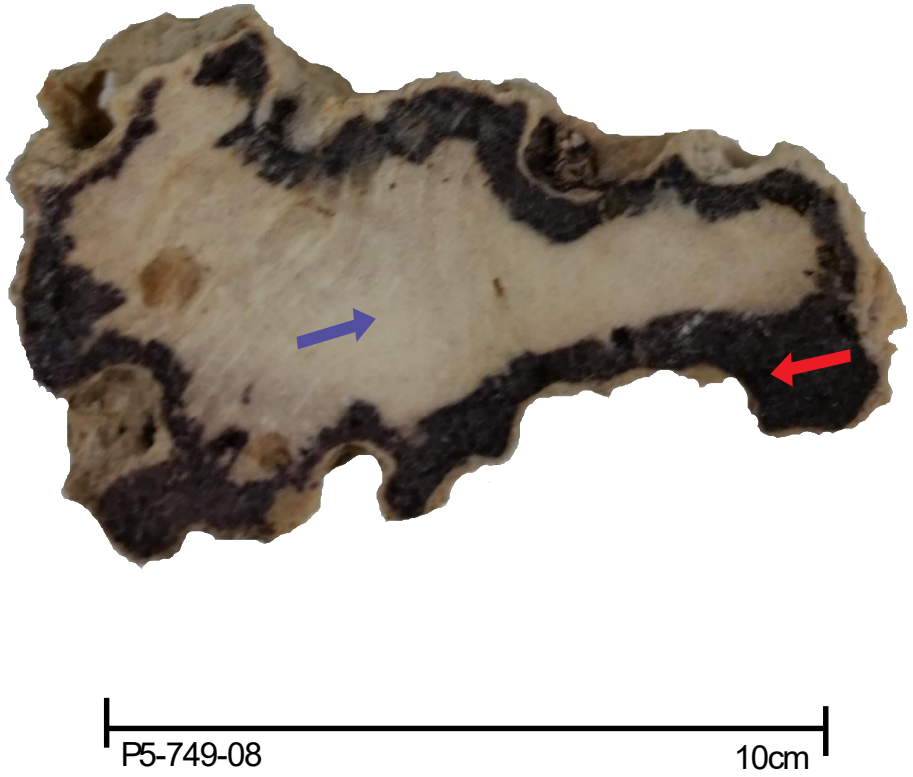

Figure 7. P5-749-08 is a Category 3 – Sponges - specimen. The dark area within the specimen is the sponge. The red arrow pointing towards it indicates the altered/non-pristine section. This section has well-formed coral skeleton but is "stained" by the presence of the sponge. The pristine section of this specimen is denoted by the blue arrow. Although there is good coral skeleton and not visibly altered, this pristine section is not as pristine as some other specimens.

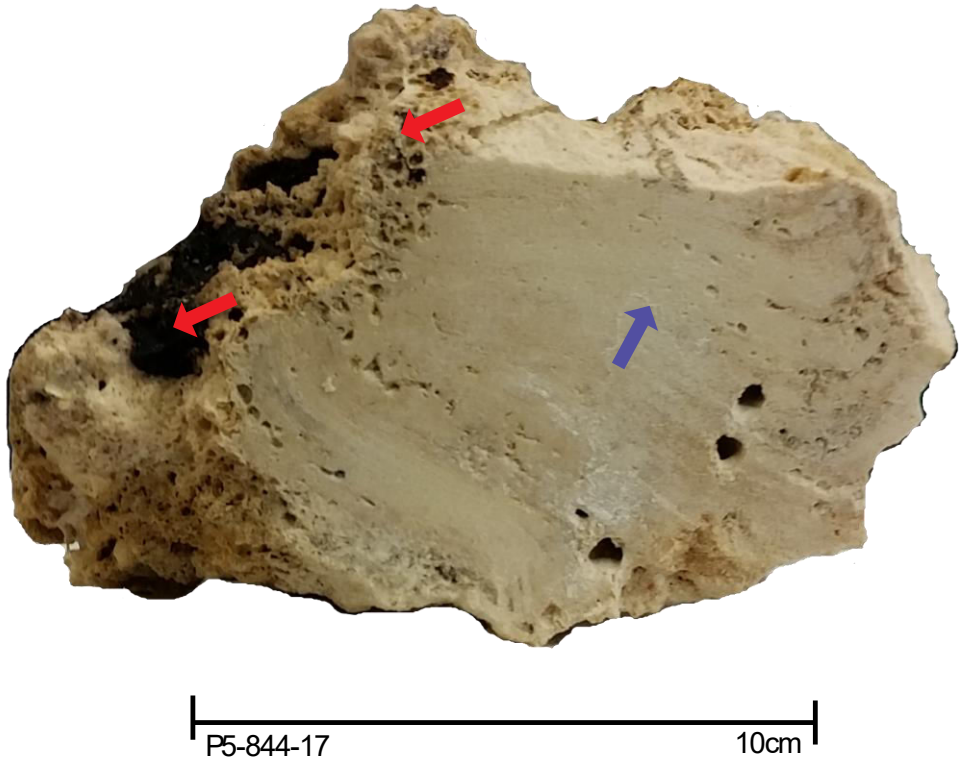

Figure 8. P5-844-17 is Category 3 – Sponge – specimen. This sponge is found attached to the outside of the specimen. The red arrows show where the altered parts due to the presence of this sponge are. The blue arrow points towards the pristine section. This section has well-formed coral skeleton but also does have some visible secondary cementation which creates the slight banding effect seen.

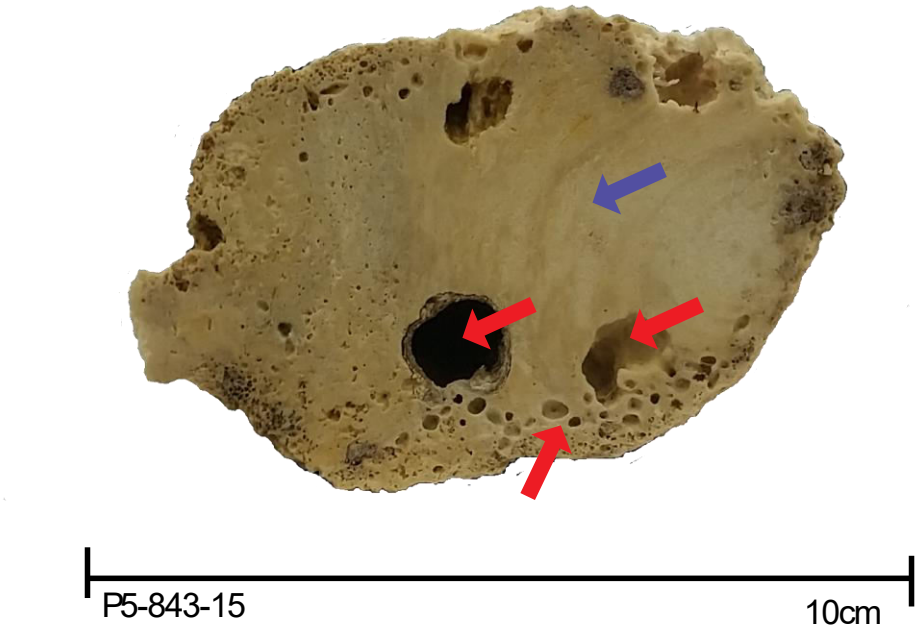

Figure 9. P5-843-15 is Category 4 – Bioerosion – specimen. The boreholes are easily seen in hand sample (pointed to by red arrows). Organic material leftover from organism can be seen in the largest borehole in the middle of the specimen. The left-hand side of the specimen is a mixture of secondary cement and hard sediment cover. The pristine (blue arrow) has some visible secondary cementation, but well-formed coral skeleton.

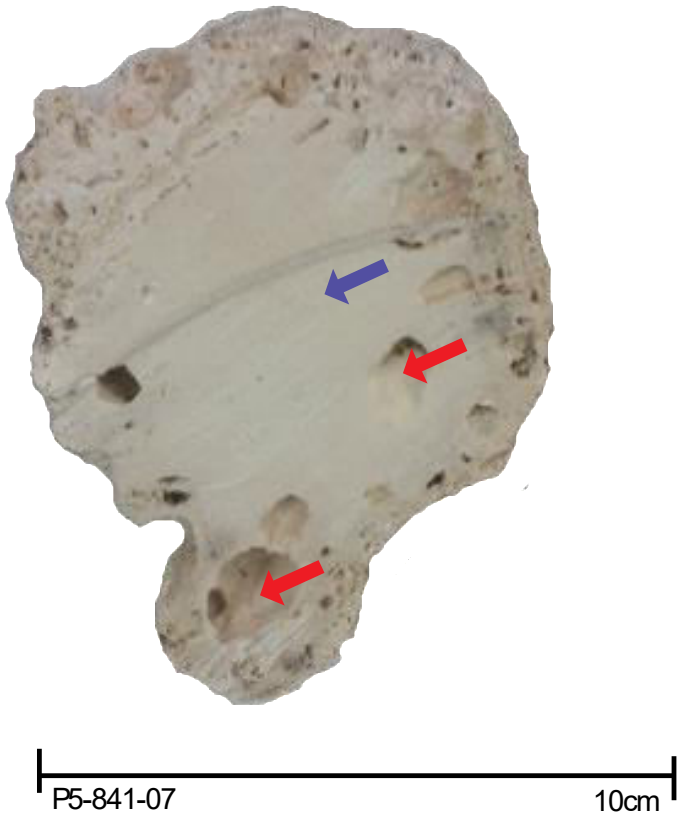

Figure 10. P5-841-07 is Category 4 – Bioerosion – specimen. The boreholes (red arrows) are in the middle of the coral skeleton; however the skeleton around it is well-formed and mostly pristine (blue arrow)

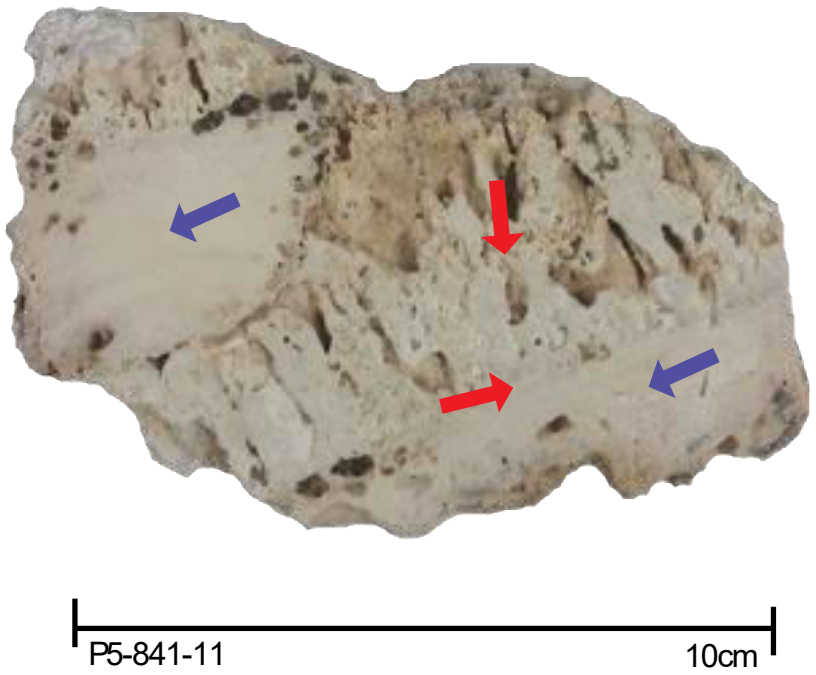

Figure 11. P5-841-11 is Category 2 – Crustose Coralline Algae – specimen. The CCA (red arrows) is seen along the coral (blue arrows) edge as well as between the two pieces of coral. It makes a fingering like shape with calcitic sediment that holds these two pieces of coral together

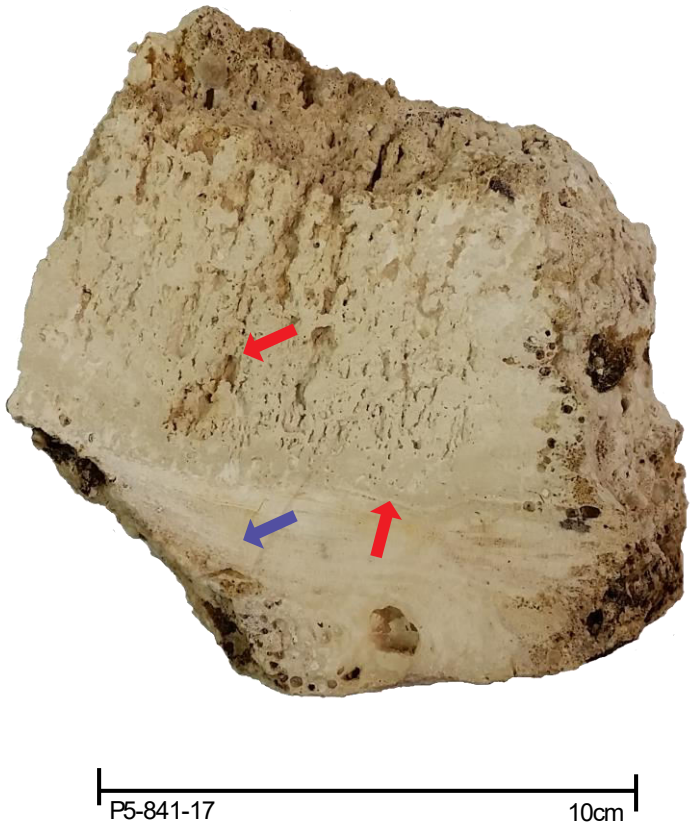

Figure 12. P5-841-17 is Category 2 – Crustose Coralline Algae – specimen. The CCA (red arrows) forms a similar morphology in this specimen as well. It is slightly layered along the contact of the coral (blue arrow) and as it interacts with the calcitic sediment becomes more of a finger-like morphology.

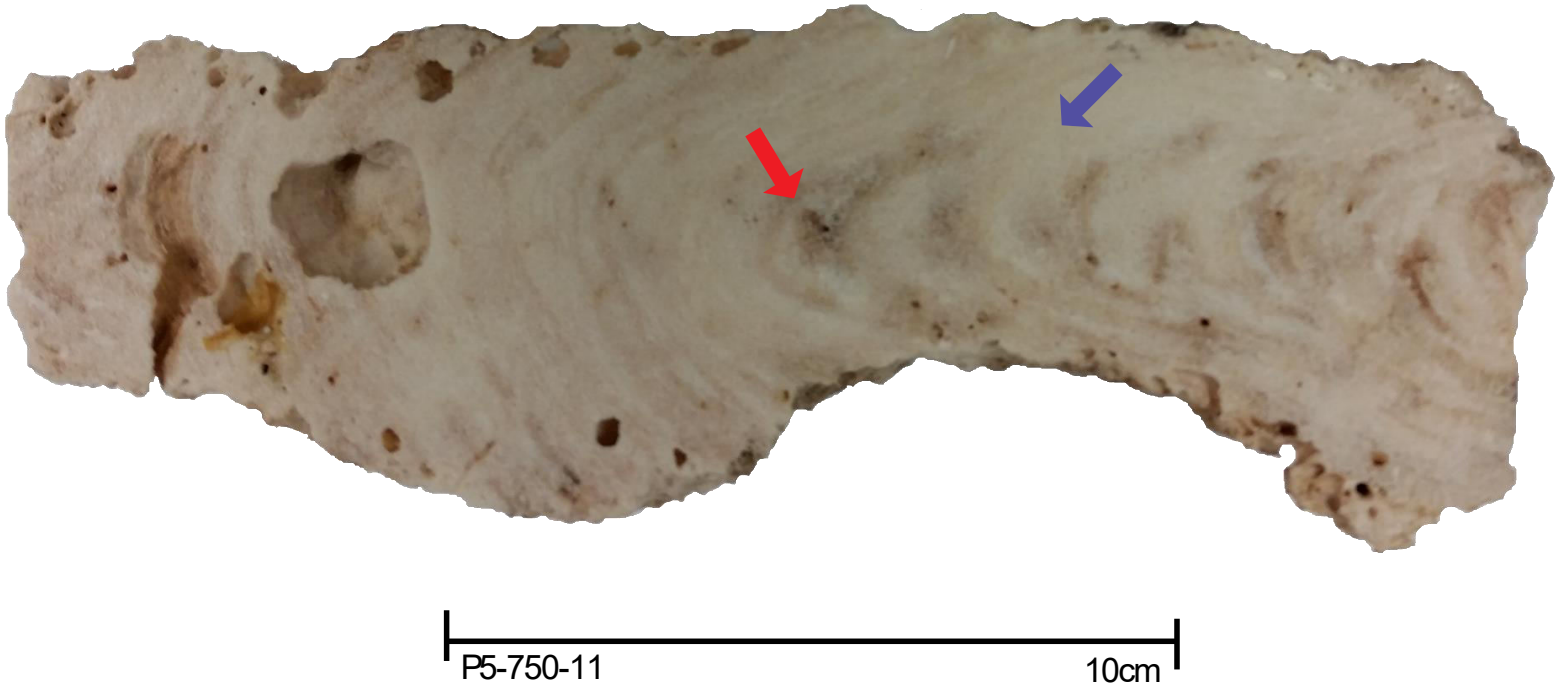

Figure 13. P5-750-11 is Category 5 – Discoloration – specimen. The discoloration (red) can easily be seen as the reddish brown hues within the coral specimen. This is detrital material filling in the pore spaces. The pristine section (blue) is any part of the coral that does not have detrital material.

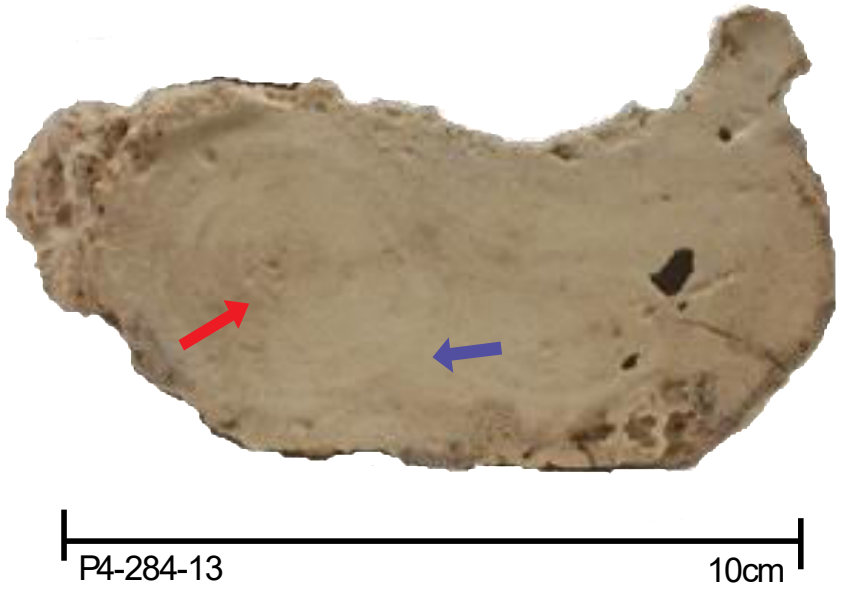

Figure 14. P4-284-13 is Category 5 – Discoloration – specimen. The discoloration (red) can easily be seen as the reddish brown hues within the coral specimen. This is detrital material filling in the pore spaces. The pristine section (blue) is any part of the coral that does not have detrital material.

From here on, “specimen” will be used to describe the complete hand sample and “sample” will be used to describe the different components and analyses of any given specimen. The specimens were subsampled into pristine and non-pristine samples. A pristine sample macroscopically appears to be largely pristine in all or part of their interiors (discernable skeletal structure, visual lack of secondary precipitates and/or extensive discoloration). Non-pristine samples are, upon macroscopic examination, visibly altered parts of skeleton at most 2m from the contact of the main alteration.

7.2 Analytical Techniques

7.2.1 Electron Microprobe

A section of the specimen that contained both pristine and non-pristine qualities was identified. This section was measured 4 mm x 2 mm for the creation of thin sections. The billets for the thin sections were longitudinal cuts along the coral skeleton. This cut is parallel to the growth axis of the coral. This allows us to determine the changes manifest within the coral skeleton as it grows Each specimen was cut with a diamond blade rock saw to thin section billet size, impregnated with epoxy, and polished into 30 um thin sections at University of Hawai‘i at Mānoa.

Element	*Line*	*Acquisition Order*	*Crystal*	*Detector*	*On-peak count time (s)*	*Off- peak count time (s) (only for one BG measurement)*
Ca	k-alpha	only	PET	Xe-sealed	50	25
Mg	k-alpha	only	TAP	gasflow	50	25
Fe	k-alpha	first	LiF	Xe-sealed	30	15
Mn	k-alpha	second	LiF	Xe-sealed	20	10
Sr -1	l-alpha	only	PETH	gasflow	40	20
Sr-2	l-alpha	second	TAP	gasflow	20	10
Si	k-alpha	first	TAP	gasflow	20	10

Table 2. The parameter settings for each element analyzed on the Electron Microprobe.

Major and minor element (Ca, Mg, Fe, Mn, Sr, Si) compositions of the primary aragonite skeleton and cements were measured on a field-emission gun electron microprobe (JEOL JXA-8500F) equipped with 5 tunable wavelength dispersive spectrometers, using Probe for EPMA software version 10.9.9 (Donovan et al., 2015). Parameter settings for both point analyses and distribution maps were: 15 keV acceleration voltage, 10 nA beam current, and 10 µm defocused beam diameter.

The usual coral composition is around 54 wt% CaO, 0.15 wt%MgO, and 0.9 wt% SrO. Analyses for Fe, Mn, and Si were below the detection limit (<0.001 wt%). Si was used to determine if there was any contamination during the thin section creation or fine-grained silicate influx in the coral pores.

X-ray intensities were acquired for Ca, Mg, Fe, Mn, Sr, and Si using the measurement conditions listed in Table 2. Each X-ray intensity acquisition consisted of peak intensity measurement followed by a background noise measurement on both sides of the peak. Net count ratios were calculated by subtracting the linearly interpolated background intensity from the peak intensity.

Standards	*Elements*					
Calcite USNM 136321	CaO	MgO	FeO*	MnO	SrO	Si*
Average Measured Standard as Unknown	56.18	0.004	0.011	0.13	0.032	0.01
2σ	0.17	0.003	0.013	0.011	0.008	0.012
Published Standard	55.84	0.0036	0.012	0.090	0.090	0.011
Dolomite USNM 10057	CaO	MgO	FeO*	MnO*	SrO*	Si*
Average Measured Standard as Unknown	30.78	21.67	0.069	0.018	0.030	0.021
2σ	0.11	0.11	0.013	0.011	0.006	0.009
Published Standard	30.40	21.75	0.01	0.008	0.023	0.018
** Published standard value for this element is based off of previous electron probe tests performed by Kate Herries*						

Table 3. Measured standards compared to published stands. All reported in wt%.

The standards used were Smithsonian Institution microprobe standards USNM 117733 Diopside (Natural Bridge, NY) for Si kα, USNM 136321 Calcite (unknown location) for Ca kα, USNM 10057 Dolomite (Oberdorf, Austria) for Mg kα, Rhodochrosite for Mn kα, NMNH R-10065 Strontianite (Oberdorf, Austria) for Sr lα,, and NMNH R-2460Siderite (Ivigtut, Greenland) for Fe kα (Jarosewich et al., 1980, Jarosewich and MacIntyre, 1983, Jarosewich and White, 1987). USNM 136321 (calcite) was within error of the published value for Ca and Mn. Fe, Mg, and Si were under the detection limit of 0.01 wt%, 0.003 wt%, and 0.01 wt%, respectively. USNM 10057 (Dolomite) was within error of the published value for Mg, Fe, and Sr. Mn and Si were under the detection limit. A comparison of the average external standard measurements and the published standard values is listed in Table 3.

7.2.2 U-Th Geochronology

Samples were prepared and analyzed following methods described in Rubin et al.(2000) and Sherman et al. (2014). Pea-sized sample chips (about 200-250mg) were chiseled from clean coral clasts. An equivalent amount of sample chips were taken from dirty sections of the same corals. After samples were selected, they were washed in a clean glass beaker with 18 megaOhm water in a sonic bath for 5 minute intervals until the water was clear. Excess water was pipetted out and the samples were dried in an oven at 60°C. Pieces were inspected under a binocular microscope and any areas of discoloration or recrystallization were removed with a Dremel tool or hand tools. The cleanest samples from both “unaltered” and “altered” portions were taken. The samples were then transferred to a Teflon beaker under clean air and a basic 15% H_2O_2 solution (equal amounts of 30% H_2O_2 and water, plus 1N NaOH) was used to leach the samples for 20-30 minutes in a sonic bath (Shen and Boyle, 1988). This was repeated if the reaction remained vigorous. Cleaned chips were then rinsed in ultra-pure, quartz sub-boiling distilled

water (QED) three times and sonified for a few minutes. The samples were finally rinsed with 0.1N HNO_3 for no longer than 30 seconds and rinsed with QED three times again. The cleaned chips were dried in filtered air before proceeding to dissolve them.

Table 4. Sample and Spike Weights (g)

Sample	Total sample weight	ID split	233U spike	IC split	229Th spike
841-17C	0.20863	0.00067	0.03492	0.20196	0.04230
841-17D	0.21266	0.00069	0.03304	0.21197	0.04222
843-15C	0.24017	0.00079	0.03484	0.23938	0.04244
843-15D	0.22558	0.00076	0.03486	0.22481	0.04233
844-17D	0.20917	0.00046	0.03477	0.20871	0.04230
749-08C	0.23866	0.00063	0.03386	0.23803	0.04237
749-08D	0.24483	0.00075	0.03510	0.24408	0.04237
841-07C	0.25258	0.00085	0.03579	0.25173	0.04252
841-07D	0.20989	0.00055	0.03539	0.20934	0.04241
841-11C	0.21247	0.00054	0.03533	0.21193	0.04244
841-11D	0.22268	0.00061	0.03544	0.22207	0.04250
284-13C	0.23313	0.00067	0.03867	0.23246	0.03960
284-13D	0.24425	0.00068	0.03616	0.24286	0.04011
750-11C	0.22249	0.00054	0.03613	0.22140	0.04008
750-11D	0.25618	0.00072	0.03628	0.25469	0.04019
844-17C	0.21211	0.00044	0.03625	0.21114	0.04018
750-07C	0.21766	0.00059	0.03621	0.21649	0.03945

Table 4. Sample split and spike weights (g). The total weight and split weights are dry weights; whereas, the spike weights are wet weights. Total sample weight should be in between 0.2-0.25g. 233U spike should be about 0.035 g or 35µL. 229Th should be around 0.040g or 40µL. Sample names are denoted as “clean” (pristine) and “dirty” (non-pristine)

Th and U were separated and purified from the dissolved bulk sample by anion exchange methods in the SOEST Isotope Lab. Samples were transferred into pre-weighed Teflon beakers and the samples were weighed until an accurate weight, 0.2-0.25g of dry sample (Table 4), was determined. All reagents were ultrapure, prepared by sub-boiling distillation, and blanked to assure acceptably low levels of Th and U before being used. Dissolution used standard procedures in our lab (e.g., Rubin et al., 2000, Sherman et al., 2014). After dissolving samples in, first in dilute HNO3 and then in7-8N HNO3, they were centrifuged to remove any insoluble (non-carbonate) material. Only one sample (P5-844-17D) had insoluble material (0.0002g) removed before splitting. Solutions were split for uranium isotope dilution analysis chemistry and U isotope composition and thorium isotope dilution and composition analysis chemistry. Based on an assumption of about 2.5ppm of U in each sample, a split containing about 1-2ng of U was taken for U ID from each sample solution, meaning about 0.002% (10 uL) of total solution. The rest was used for U IC and Th ID/IC analysis. U ID splits were spiked with calibrated 233U, and Th splits were spiked with calibrated 229Th. Each spiked split was equilibrated, evaporated to dryness, then converted and dissolved into 200uL of 7.5N HNO3 for Th and U separation.

The solutions were separated through an anion exchange resin in quartz glass column for IC splits and through Teflon columns for ID splits. ID resin was pre-cleaned in large batches before use. For ID columns, anion exchange resin was washed with 8N HNO3 and checked for Cl- with $AgNO_3$. U Isotope dilution (ID) was eluted off about 500uL of 200-400 mesh AGI-x8 Eichrom Resin, kept in chloride form. The columns were conditioned with 2-3mL of 7-8N HNO3 in order to convert to nitric and checked (using the wash acid) for chlorides using $AgNO_3$, which will form an AgCl precipitate if any Cl- are present in columns. Samples in 200uL

solution of 7-8N HNO3 were gently loaded onto the resin and allowed to drip through. The sample and resin was washed with 2 mL of 7-8N HNO3 in steps of 500uL, 500uL, and 1000uL. The wash was collected into the original beaker and kept for later Sr chemistry. The resin was then washed with two round of 125uL of highly purified water (QED). Finally, U was eluted off 3mL (250uL, 250uL, 500uL, 1000uL, 1000uL) of 1N HBr which was collected into a clean beaker. The solutions were dried down completely and brought back up in 50 uL of 7-8N HNO_3. This step was completed twice in order for the solution to be fully converted to HNO_3. Then the final solution was dried down to 2-3uL to prepare to load.

Th IC/ID and U IC were separated using anion exchange (AGI-x8 100-200 mesh) resin. Quartz glass columns stored in 2N HNO_3 were sonified for 30 minutes in 4N HNO3 and then 10 minutes in 18 megaohm Millipore. The cleaned columns were set up in a clean-air hood and washed with QED. We filled the columns with 3mL of wet AGI-x8 100-200 mesh resin. The resin, kept in chloride form, for this procedure was not pre-cleaned before being loaded on the column. It was washed with 18mL (1mL, 1mL, 1mL, 15mL) of 6N HCl, then 3mL (1mL, 1mL, 1mL) QED, and finally 24 mL (3mL, 21mL) of 0.5N HNO_3. The columns were covered and let to sit overnight. The following day, we conditioned the columns with 6-9mL (in 3mL increments) of 7-8N HNO3 in order to fully convert the resin to nitric form for sample loading. After each 3mL, we checked the wash acid for chlorides with $AgNO_3$, which will form an AgCl precipitate if any Cl- are still in resin. Once confirmed free of chlorides, the samples, in 200uL of 7-8N HNO_3, were gently loaded onto the column and allowed to drip through. We washed the sample and resin with 10mL (1mL, 1mL, 1mL, 1mL, 3mL, 3mL) with 7-8N HNO_3. The wash was collected into the original beaker. Setting a new beaker labeled “Th ID/IC” underneath the column, we washed the column with two round of 250uL QED. Th was eluted off with 12mL

(1mL, 1mL, 1mL, 3mL, 3mL, 3mL) of 6N HCl. A new beaker was set up labeled “U IC.” Then U was eluted off with 12mL (1mL, 1mL, 1mL, 3mL, 3mL, 3mL) of 1N HBr.

Each solution was dried down, converted to nitric form using 50uL steps, refluxed with a solution of 50uL 30% H_2O_2 and 50uL 7-8N HNO_3 to rid any organics from resin, converted back to nitric, then dried down. The Th ID/IC samples were brought up in 200uL 7-8N HNO3 to prepare for a clean-up column. The U IC were brought back up 0.5N HNO3 to prepare for analysis as a solution, by MC-ICP-MS.

Th ID/IC splits were brought through a clean-up anion resin column to further purify from U as well as remove any resin that bled off from the first column into the sample beaker. After the conversion to nitric, the samples we brought back up in 200uL of 7-8N HNO3. Teflon columns were stored in 3N HCL and set on a hot plate overnight (not boiling). The columns were then sonified in new 3N HCL for 30 minutes, rinsed 3x with QED, and sonified in QED for 30 min. All bubbles that formed in the columns were removed before sonifying. The columns were set up in a clean-air hood. Each column was filled with 500uL of wet AGI-x8 200-400 mesh resin and washed with 1mL QED. The columns were conditioned with 2-3mL of 7-8N HNO_3. After each mL, we checked for chloride ions in the wash using $AgNO_3$. Once confirmed free of chloride ions, the samples were gently loaded in 200uL 7-8N HNO_3 and allowed to drip through. The resin and sample were washed with 2mL (500uL, 500uL, 1000uL) of 7-8N HNO_3. This wash was collected into the same “Th wash” beaker from the previous columns. We put the now empty beaker labeled “Th IC” under the columns to collect the eluted Th. The column was washed 2x with 250uL of QED. Th was eluted off with 2mL (250uL, 250uL, 500uL, 1000uL) of 6N HCl. The solution again was dried down, converted to nitric, refluxed with a solution of 50uL 30% H2O2 and 50uL 7-8N HNO3, converted back to nitric, then dried down to 4-5uL.

The purified U and Th fractions were reduced to approximately 2-3uL by gentle heating prior to loading on ultra-cleaned Aquadag carbon mixed with QED onto outgassed single high purity, zone-refined Re metal filaments. The U isotope dilution was run at temperatures between 1700-2000°C and at currents between 4.00-4.20A (variable from sample to sample) on the VG Sector 54 Thermal Ionization Mass Spectrometer at the University of Hawai‘i at Mānoa. First, we brought up the high tension on the machine. Then the filaments are warmed up either by hand or using a pre-set program. At a filament current of 3.25A, the line of sight is opened and the detector is switched to Daly. We changed the focus of the ion beam and raise the filament current to bring the intensity of mass 238 beam up to at least 0.3mV (16000cpm) and intensity of mass 233 up to 0.03mV in order to run the samples. The analyses are conducted in a single-collector mode by peak-jumping on a Daly ion-collector. Masses 233, 235, 238 and the baseline are measured on peak for 10 seconds, 10 times per block. Linearity of the ion counter is within counting statistics everywhere within the range of 10 cpm to $2x10^6$ cpm. The sample is run to a sufficient error (<0.05 % standard error, usually 0.025%). Data acquisition takes 2-4 hours and 100-200 ratios.

The Th isotope dilution and isotope concentration was run at temperatures between 1950-2200 °C and currents between 4.30-4.70A (variable from sample to sample) on the VG Sector 54 Thermal Ionization Mass Spectrometer at University of Hawai‘i at Mānoa. First, we brought up the high tension on the machine. Then the filaments were warmed up either by hand or using a pre-set program. At a filament current of 3.25A, the line of sight is opened and the detector is switched to Daly. We change the focus of the ion beam and raise the filament current to bring the intensity of mass 229 beam up to 0.2mV and intensity of mass 230 up to 0.0002mV in order to run the samples. The analyses are conducted in a single-collector mode by peak-jumping on a

Daly ion-collector. Masses 229, 230, 232 and the baseline are measured for 5 seconds 10 times per block. Linearity of the ion counter is within counting statistics everywhere within the range of 10 cpm to $2x10^6$ cpm. The analyses were run to exhaustion.

U isotope composition was analyzed on the Nu Plasma Multi-Collector HR Mass Spectrometer at the University of Hawai‘i. Instrument calibration of 5ppb, 10ppb, and 20 ppb CRM112a U std solution were run. The sample solutions were brought up in a known mass of 10% in 100uL of 0.5N HNO_3, and ^{238}U intensity measurements were quickly taken. U concentrations for the sample solutions were determined using the CRM112a calibration curve. Then sample solutions were diluted down to the target U concentration of 5ppb U. This concentration was chosen to preserve the Ion Counter detector used for the measurement of ^{234}U. After the instrument was tuned, a sample solution of CRM112a was run. After the preceding bracketing standard run, the inlet system was rinsed for 7-10min with 0.5N HNO_3. This is more than sufficient to reduce the ^{238}U intensity to less than 1 permil of its intensity during a standard or sample run. After the rinse and the first standard, we run another standard, which starts the normal procedure. The full analytical procedure was standard – rinse – sample – rinse – standard – rinse. The analytical routine consisted of 3 blocks of 24 measurements, and each measurement was comprised of 2 cycles. Peak centering on ^{238}U was performed for each of the two cycles at the beginning of every block. Zero measurements for baseline correction were taken for 10s at the beginning of each block. Zeros were done by ESA deflection. The first analytical cycle took data for 5s (^{238}U in L1, 235U in L5, 234U in IC0). The second analytical cycle took data for 3s (^{238}U in L2 and 235U in IC0). Each magnet jump also included 2s of setting time. Each run takes approximately 20 min to run. 235U from the two cycles was used to correct for detector gain drift between IC0 and L5, Mass bias and IC-Faraday gain was corrected on each cycle by

235U/38U normalization to 0.0072527, and then additional mass bias correction was done using the mean of he before and after bracketing standard.

The absolute age of the fossil coral was determined using the ^{230}Th-^{234}U-^{238}U technique. Standard isotope dilution methods were used. The U ID/IC and Th ID/IC data was manually reduced in a spreadsheet.

2.2.3 Duplicate Analyses

Many duplicate U and Th analyses were run using the second half of the same digested solutions. The duplicated analyses are noted in Table 5.

8. Results

8.1 Samples

8.1.1 Hand Sample

Each specimen is visually different in concern to alterations (Section 7.1.2). The main coral skeleton – or the primary aragonite – is intact and easily seen in hand sample for each specimen.

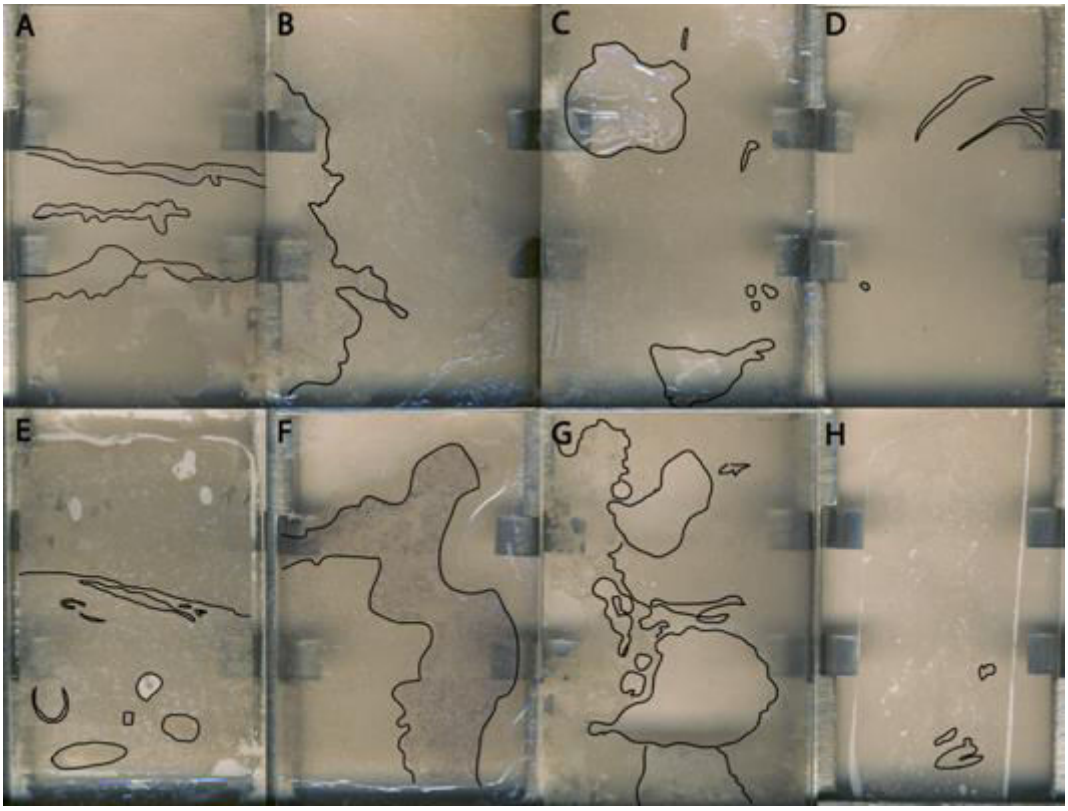

Figure 15. Visible alterations in thin sections are outlined in black. A and E are both specimens overgrown with crustose coralline algae and calcitic sediment (top and bottom sections of A and top section of E). Secondary cements are visible and abundant closer to the crustose coralline algae. E does have some bivalves present in the coral skeleton. B and F have sponges present (left side of B and purple coloring in F). There is secondary cement present in both samples, but are difficult to see in this image. C and G have been affected by bioerosion. Multiple large boreholes are present in both specimens. The left side of G is porous calcitic sediment; whereas, around the boreholes themselves is secondary cementation. D and H have discoloration in the hand sample. The discoloration is not visible in this image, however, some secondary cementation is.

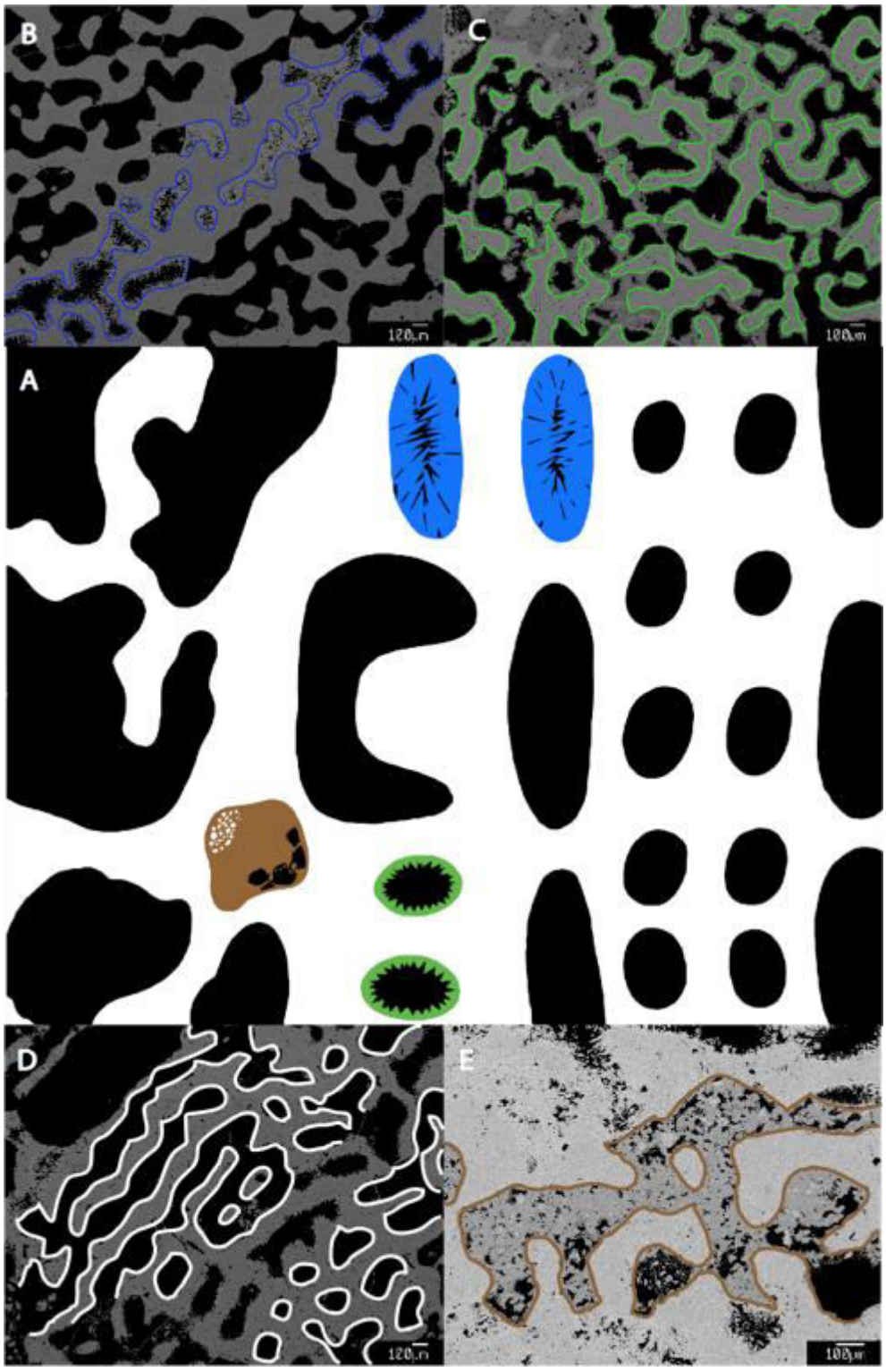

Figure 16. A) Schematic of an average coral skeleton seen in both optical microscope and electron microprobe backscattered electron images. The colors in the schematic correlate to the colors in the backscattered electron images: blue (B) - secondary aragonite cement, green (C) - secondary calcite cement, white (D) pristine primary aragonite skeleton, brown (E) - calcitic infilling of pores usually created from secondary calcite cement and can have chips of aragonite skeleton within.

8.1.2 Primary Aragonite

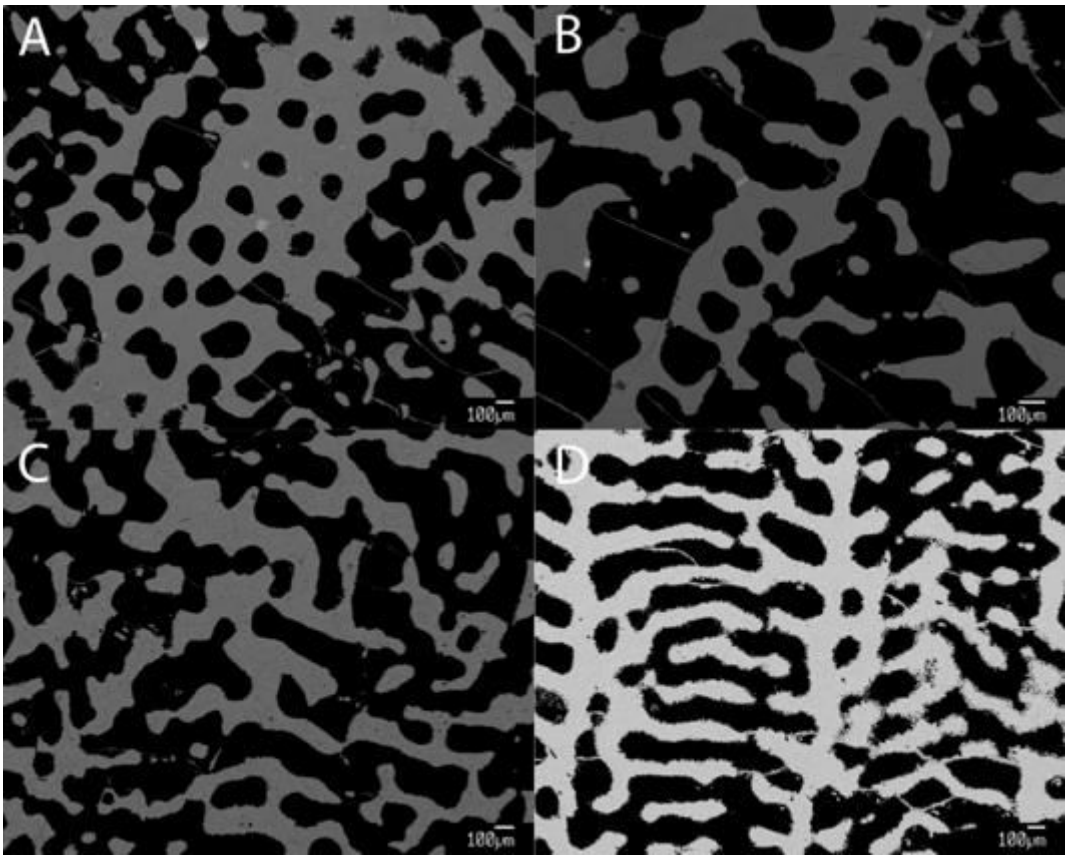

Figure 17. Backscattered Electron Images of pristine primary aragonite skeleton. The grey is coral skeleton. Black is pore space filled with epoxy. The difference in color between photos is due to a mechanical difference in the brightness of the electron microprobe imaging software. Primary aragonite is considered pristine when there are no secondary cements present. The shape and structure of the primary aragonite is created by the coral while growing and is typical for a *Porites sp*.

The primary aragonite skeleton is compositionally homogeneous. The average skeleton for all specimens has about 54.6±0.097** wt% CaO, 0.14±0.004 wt% MgO, and 0.89±0.012 wt% SrO (n=503; where ± equals two sigma uncertainty). Mg/Ca, on average, was 3-4 mmol/mol, and Sr/Ca was 9-10 mmol/mol. The table below shows the average skeletal makeup of the eight individual specimens in the study.

8.1.3 Secondary Cements

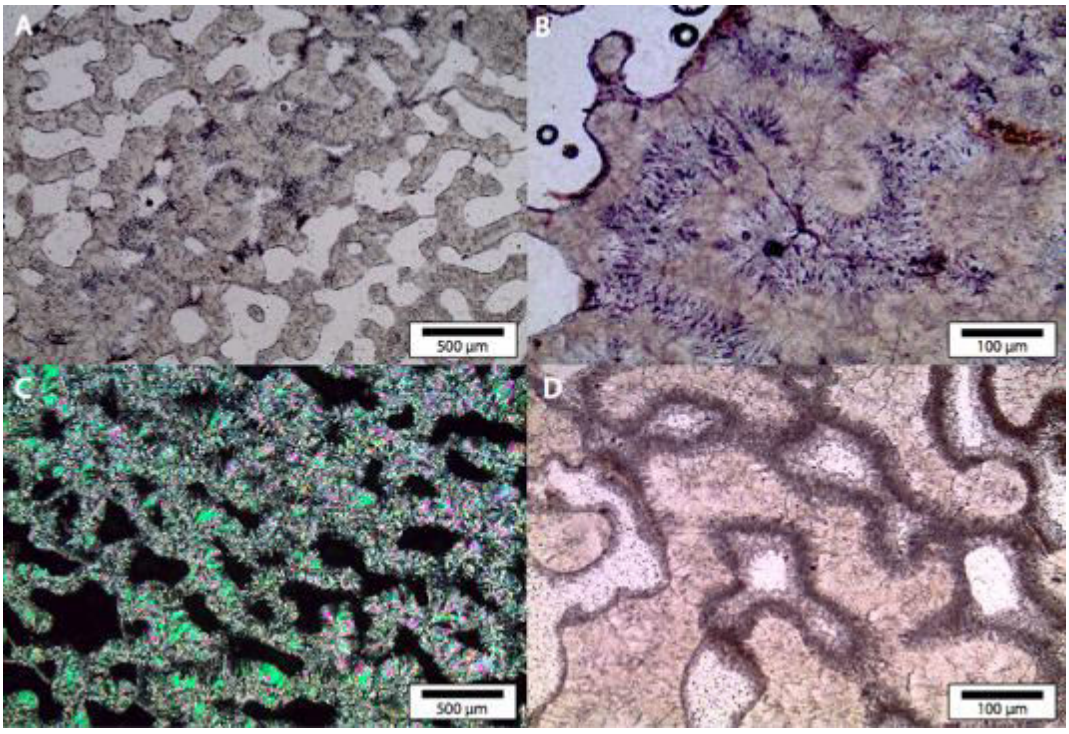

Figure 18. Three (A,B,D) plain-light and one (C) cross polarized- light photomicrographs of the secondary cements present. A and B are secondary aragonite cement, which is defined by long, acicular needles. C and D are Mg-calcite cement which forms shorter, isopachous crystals.

The samples have first-generation shallow-marine aragonite and Mg-calcite cements. The aragonite is found as long, acicular needles (Figure 18) whereas the Mg-calcite forms shorter, isopachous crystals. Both cements are typical shallow marine reef cements (Ian G. MacIntyre, 1977). The distribution of cements is heterogeneous, and we observe large variations in the abundance and types of cement within even single coral thin sections (Figure 19). Similar small scale spatial variation has been reported in other studies (Allison et al., 20070). Figure 19 shows the percent of each type of cement in each specimen. For most samples, pristine primary aragonite dominated, except for 841-07 and 844-17 which either had more or close to equal amounts of secondary cementation. Secondary aragonite percentage was greater than secondary calcite except for 841-17 and 844-17. 284-13 and 750-11, the two discoloration samples, had the

lowest amount of secondary cement other than the totally pristine sample 750-07. The two specimen (841-17 and 841-11) which have crustose coralline algae have the greatest variation in the three different components. The amount of secondary calcite in these two specimen increases towards the contact between the coral skeleton and the crustose coralline algae. For the bioerosion specimen (843-15 and 841-07), the amount of secondary aragonite tends to increase near the boreholes, though there is secondary cementation throughout the whole area. The discolored samples show no visible pattern or predictable variation in the amount of cementation. The two sponge specimens vary dramatically between each other. 844-17 has secondary calcite, which is mostly concentrated around the contact of the sponge and coral. For 749-08, there is no visible pattern, with secondary aragonite occurring in both the pristine and non-pristine parts of the skeleton.

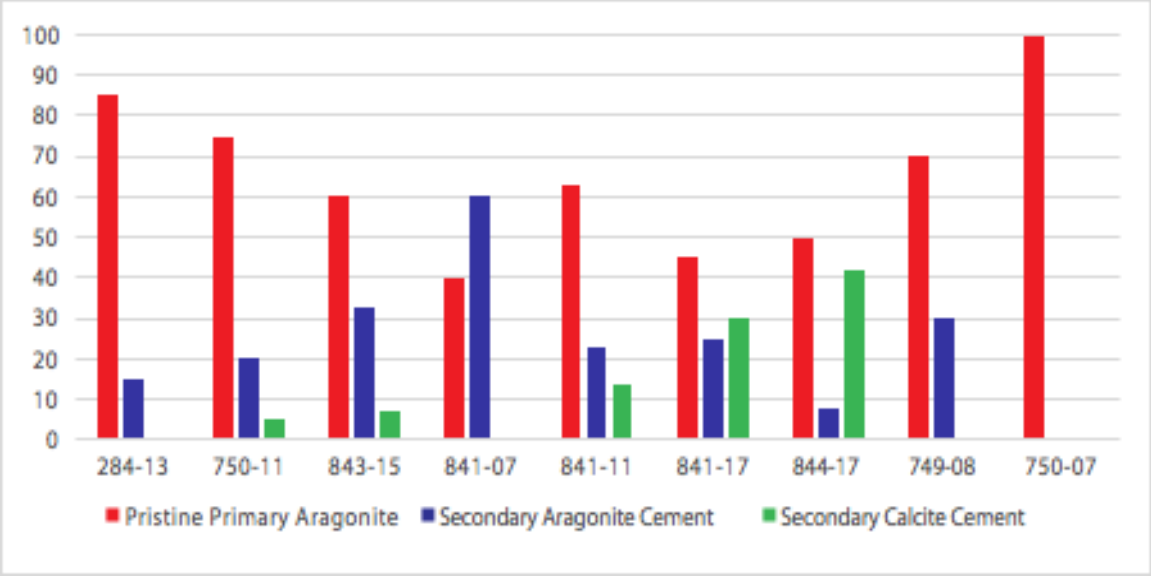

Figure 19. This table shows the percentage by area of each thin section that is pristine primary aragonite, secondary aragonite cement, or secondary calcite cement. The percentages were calculated using observations from both petrographic microscope and electron microprobe work. Pristine primary aragonite was only considered if the skeleton showed no cementation. Sections that had any cementation present were counted in the separate cement percentages.

8.1.3.1 Secondary Aragonite Cement

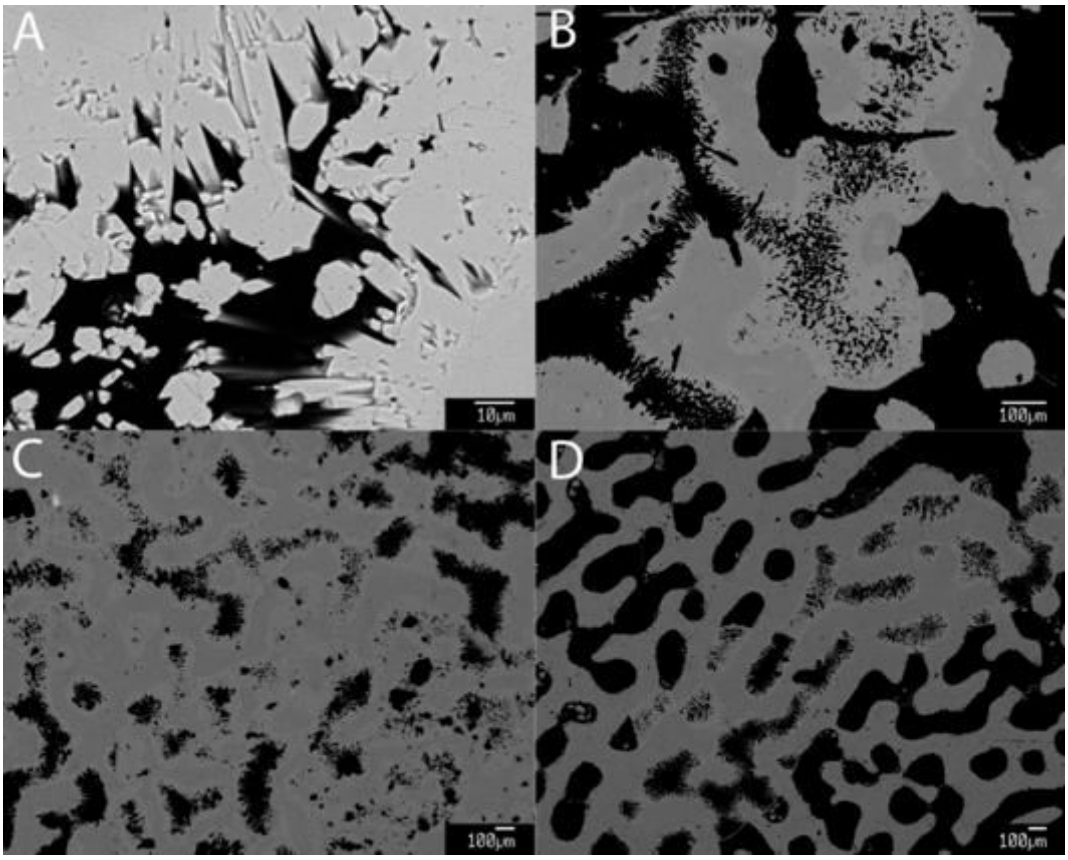

Figure 20. Backscattered Electron Images of secondary aragonite cement. A shows the crystal shape of the acicular needs and some more blocky crystals. B, C, and D all show the different ways aragonite cement can be present. In B, the cement is contained to the one small area. In C, the secondary aragonite cement is prevalent throughout the whole image. D shows the aragonite cement in a banded pattern, with pristine primary aragonite surrounding it.

The secondary aragonite cement is found in almost every single specimen, except the completely un-altered specimen (750-07). There is a range of abundance throughout the specimens from less than 10% to upwards of 60%. Within any given specimen, the secondary aragonite crystals may be thin and sparse to completely filling in pore spaces. The acicular aragonite crystals have a higher Sr content than the primary aragonite (Figure 20), averaging about 11 mmols/mol Sr/Ca. The Mg content is significantly lower than both skeleton and Mg-calcite cement. This enrichment of Sr and depletion of Mg is common for shallow-marine

aragonite cements (Allison et al., 2007; Ian G. MacIntyre, 1977; Lazar et al., 2004; Ribaud-Laurenti et al., 2001). If the different cements are found together, the acicular aragonite is almost always deposited first. The aragonite cement more than likely formed simultaneously with coral growth (Sherman et al., 1999).

8.1.3.2 Secondary Calcite Cement

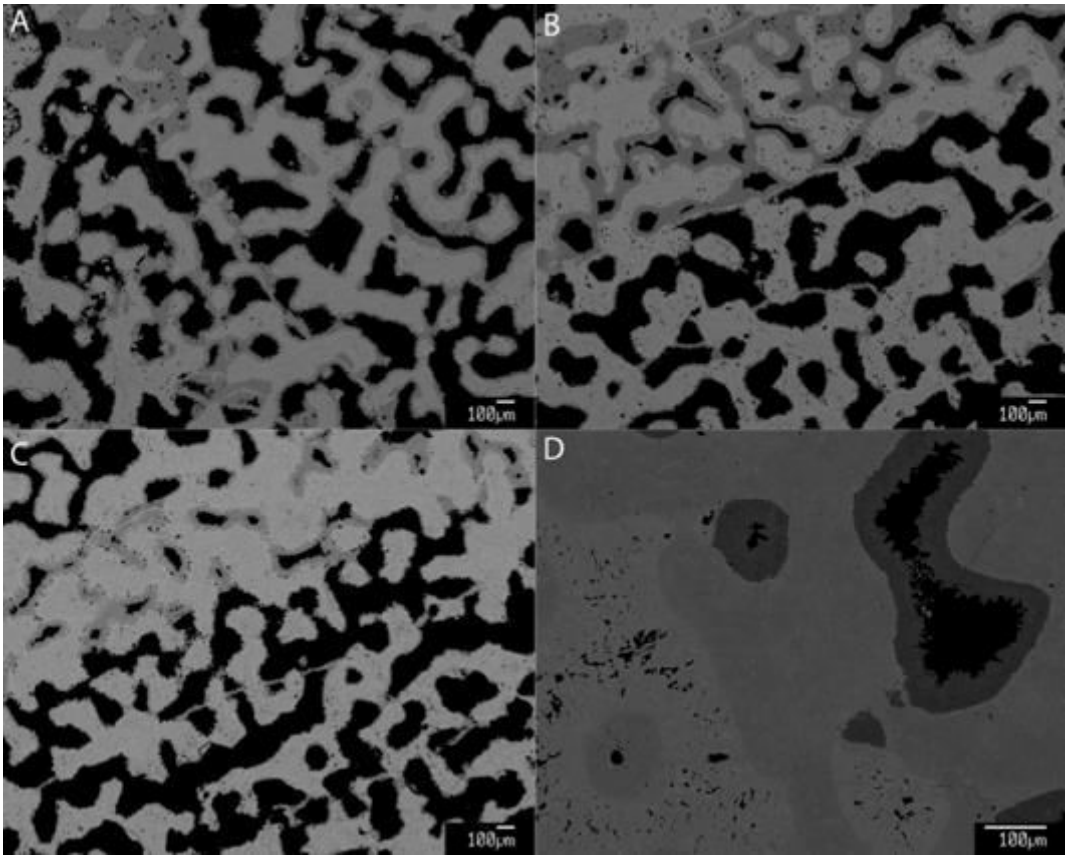

Figure 21. Backscattered Electron images of secondary calcite cement. A, B, C show various patterns of secondary calcite cement distribution. As seen in some of the pore spaces in A and B, the secondary calcite can fill in the whole pore. D compares secondary calcite cement with secondary aragonite cement. The difference in crystal shape and geochemical composition (eg mean atomic number) is apparent.

Mg-calcite cement is not as abundant in the specimens. It is usually found close to any alteration in the coral. The cement also forms as a first-generation; however, it also forms

coatings on the acicular aragonite cement. Mg-calcite cement usually occurs in a range of textures: as micrite and as steep-sided rhombs, continued growth of which produced dog tooth crystals (Lazar et al., 2004; Sherman et al., 1999). The Mg-calcite cement has enriched Mg content of 6 wt% MgO, compared to the 0.15 wt% of the skeleton (Figure 21). Mg-calcite cement can fill entire pore spaces (Figure 21). When this happens, the cement can incorporate broken pieces of coral skeleton into the matrix. Totally filled pores only occur in about 5% of all pores that have Mg-calcite cement.

8.2 General U-Th data

Absolute ^{230}Th-^{234}U-^{238}U ages were collected for 9 *Porites compressa* specimens, which consists of 17 ages total (Table 5). Data were reduced using the decay constants of Cheng et al., 2013.

Sample Name	*(234U/238U)*	*±2σ*	*(230Th/238U)*	*±2σ*	*[238U]*	*±2σ*	*[232Th]*	*±2σ*	*[230Th]*	*±2σ*	*Calculated Age*	*±2σ*	*δ234Ui*
P4-284-13C	1.135	0.003	0.155	0.002	3.09	0.004	0.913	0.002	7.8	0.0001	16015	231.1	141.48
P4-284-13C2	1.135	0.003	0.158	0.002	3.09	0.004	0.914	0.008	7.9	0.0001	16277	253.3	141.59
P4-284-13D	1.139	0.003	0.163	0.002	2.97	0.005	2.671	0.008	7.9	0.0001	16856	250.6	145.44
P4-284-13D2	1.139	0.003	0.162	0.001	2.97	0.005	2.667	0.005	7.8	0.0001	16742	141.8	145.39
P5-750-11C	1.134	0.003	0.167	0.002	3.07	0.005	0.947	0.002	8.3	0.0001	17389	243.8	140.52
P5-750-11D	1.144	0.003	0.164	0.003	3.09	0.005	1.856	0.006	8.3	0.0001	16867	299.5	151.26
P5-750-11D2	1.144	0.003	0.170	0.002	3.09	0.005	1.751	0.004	8.6	0.0001	17544	182.7	151.55
P5-749-08C	1.141	0.008	0.112	0.001	3.41	0.005	2.364	0.007	7.5	0.0001	11257	150.9	145.67
P5-749-08D	1.136	0.008	0.138	0.003	3.06	0.005	3.416	0.014	6.9	0.0001	14154	337.0	141.39
P5-844-17C	1.139	0.003	0.140	0.002	2.21	0.003	1.719	0.004	5	0.0001	14232	175.3	144.92
P5-844-17D	1.149	0.005	0.126	0.002	2.22	0.004	3.204	0.011	4.6	0.0002	12709	196.1	154.02
P5-844-17D2	1.149	0.005	0.126	0.001	2.22	0.004	3.178	0.004	4.6	0.0002	12685	149.8	154.01
P5-750-07C	1.136	0.003	0.148	0.002	3.06	0.004	0.263	0.003	7.4	0.0001	15219	179.8	141.73
P5-843-15C	1.151	0.004	0.199	0.003	2.22	0.003	0.312	0.002	7.2	0.0042	20646	276.6	160.23
P5-843-15C2	1.151	0.004	0.197	0.002	2.22	0.003	0.294	0.001	7.1	0.0001	20399	189.2	160.11
P5-843-15D	1.141	0.005	0.153	0.002	2.84	0.004	0.255	0.001	7.1	0.0001	15701	165.7	147.11
P5-843-15D2	1.141	0.003	0.155	0.002	2.84	0.004	0.258	0.001	7.2	0.0001	15951	193.9	147.21
P5-841-07C	1.134	0.004	0.153	0.001	3.07	0.003	0.294	0.004	7.7	0.0001	15824	154.4	140.04
P5-841-07D	1.136	0.005	0.153	0.002	3.30	0.008	0.596	0.007	8.2	0.0001	15745	195.1	142.60
P5-841-11C	1.135	0.003	0.129	0.001	3.70	0.007	0.512	0.002	7.8	0.0001	13193	125.0	140.38
P5-841-11D	1.139	0.003	0.134	0.002	2.91	0.005	0.934	0.002	6.4	0.0001	13673	167.2	144.11
P5-841-17C	1.141	0.003	0.226	0.002	1.97	0.002	1.380	0.002	7.2	0.0001	24056	242.1	150.46
P5-841-17C2	1.141	0.003	0.233	0.004	1.97	0.002	1.432	0.007	7.4	0.0001	24788	475.6	150.77
P5-841-17D	1.139	0.003	0.218	0.003	2.01	0.003	2.142	0.013	7.1	0.0001	23069	323.8	148.22
P5-841-17D2	1.139	0.003	0.217	0.002	2.01	0.003	2.086	0.003	7.1	0.0001	23006	252.3	148.19

Table 5. U-Th data reported according to Dutton et al., 2017. 2σ standard error reported. Concentration values reported in [brackets], activity ratios are reported in (parentheses), [^{238}U] reported in ppm, [^{232}Th] reported in ppb, δ234Ui reported in ‰.

Reruns of same dissolution Th samples are denoted in orange and by "2" at the end of the sample name .

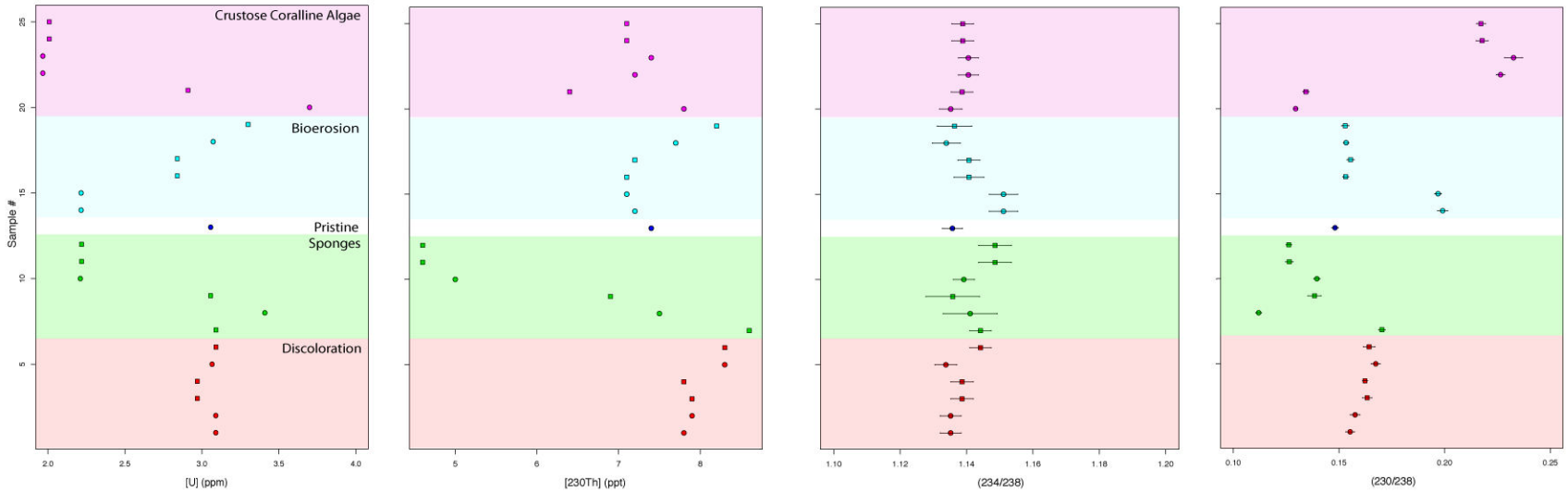

Figure 22. The three separate U-Th components that are used to calculate ages: [^{238}U],[^{230}Th],(^{238}U/^{234}U). The activity ratio of (^{230}Th/^{238}U) is also included. Each are separated into the five categories of alteration: Crustose Coralline Algae(magenta), Bioerosion (teal), Pristine (white - blue marker), Sponges (green), and Discoloration (red). Circles are pristine samples; squares are non-pristine. Second analyses of the same dissolution were conducted for [U] and [Th]. Error bars are 2 σ for (^{234}U/^{238}U) and (^{230}Th/^{238}U). Error bars for [U] and [Th] are smaller than marker size. The same marker and color scheme is used for the rest of the graphs.

The majority of our samples cluster around a uranium concentration of about 3 ppm. There are nine samples that stand out with lower [U]. The [^{230}Th] are all very similar except for 3 of the sponge samples. However, those 3 samples correlate with 3 lower U concentrations. The (^{230}Th/^{238}U) ratio for these three samples is very similar to the rest of the samples. (^{234}U/^{238}U) has the largest error of all analyses. All of the samples are within error. Lastly, the (^{230}Th/^{238}U) has variation between different categories. The Discoloration samples are within error of each other. The Sponge samples show variation. The two Bioerosion samples that have low [U] have much higher (^{230}Th/^{238}U) than the rest, same with the four samples in the Crustose Coralline Algae. Reasoning behind this difference in analyses is further explained in the text

8.2.1 (230Th/238U)

The ratio of the two isotopes ^{230}Th and ^{238}U gives us insight into the measured age of each sample before any calculations are complete. (^{230}Th/^{238}U) ratios for deglacial corals are usually in between 0.11 and 0.18 (K. Rubin, personal communication). Our samples range from 0.129-0.167±0.0015, with outliers above 0.2 (Figure 22).

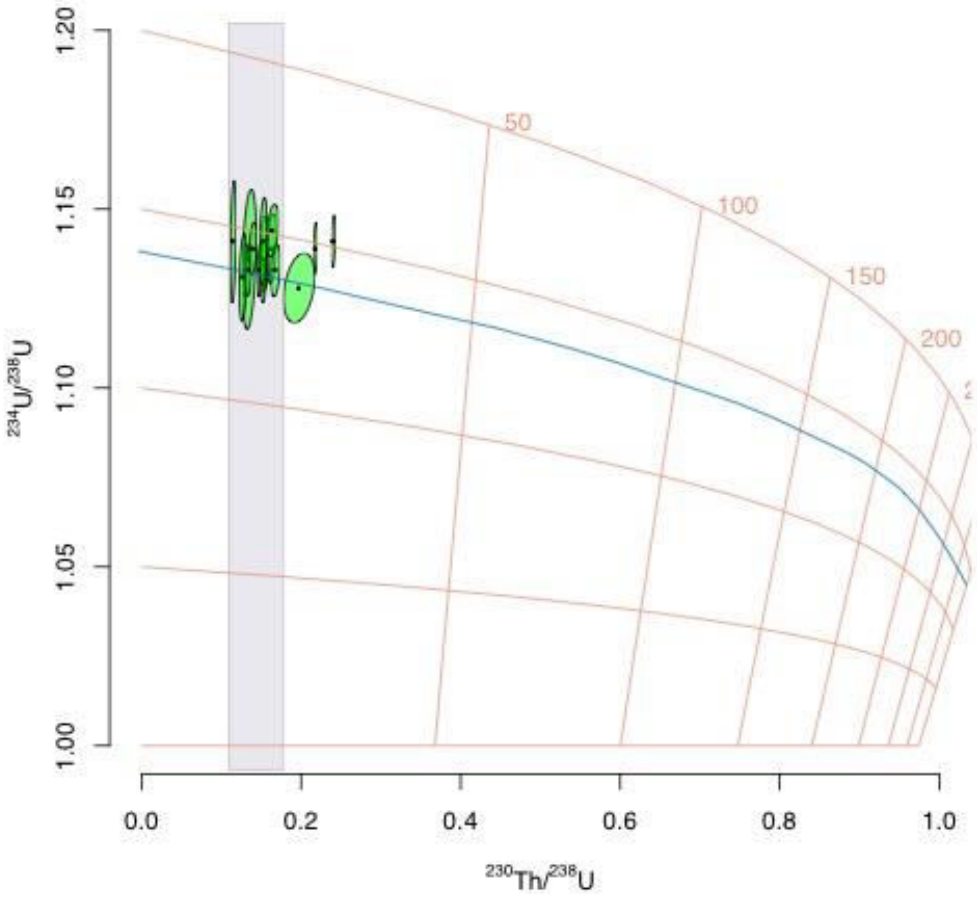

Figure 23. (^{230}Th/^{238}U) versus (^{234}U/^{238}U) plotted on a seawater evolution curve. This graph illustratess the temporal development of activity ratios in the samples under closed-system conditions with the initial (^{234}U/^{238}U) of modern seawater. A significant deviation of the initial (^{234}U/^{238}U) from the seawater value indicates potential alteration or open-system behavior and the ^{230}Th/^{238}U-age has to be considered non-reliable (Scholz and Hoffman, 2008). The blue line shows the (^{234}U/^{238}U) =1.145, whereas the horizontal orange lines show the ticked ^{234}U/^{238}U and the vertical lines show the noted age isochrons. The grey box shows the (^{230}Th/^{238}U) range deglacial corals are expected to plot. Most samples fall near the 14-15ka isochron near the 1.145 reference line.

8.2.2 (234U/238U) and δ234Ui

($^{234}U/^{238}U$) is the activity ratio of the two main isotopes of U that are used to calculate ages. When corals incorporate U into their skeleton, they incorporate U in a specific ratio of these two isotopes. Literature reports a normal seawater ratio to be about 1.145 (Cheng et al., 2013). ($^{234}U/^{238}U$) for all samples fall between 1.134 and 1.144 ± 0.003 (2 σ) (Figure 22). Most of these samples fall just below the reference line.

δ234Ui is delta-notation of ($^{234}U/^{238}U$), which is the relative difference in two isotopic ratios expressed in parts per mille (‰). In this case it is the deviation from a secular equilibrium ratio of 1.00. δ234initial is back calculated using the measured δ234, the decay constant, and the U-Th ages, in order to understand what seawater looked like while the coral was being formed and if the coral evolved over time as a closed system. δ234Useawater is normally denoted as 145‰ for previous coral/U-series studies (Hibbert et al., 2016; Sherman et al., 1999). However recent publications (Chutcharavan et al., 2018; Hibbert et al., 2016) have found a slight decrease in δ234Usw during the deglacial time period. For this study, a relative δ234Usw of 145‰ will be assumed, but the data present could possibly support this slight decrease in δ234Usw.

As seen in Figure 24, most of the Penguin Bank samples fall reasonably close to the 145‰ line within analytical uncertainty. There are four samples that have high δ234Ui. The rest of the samples fall within to statistically different groups: 141‰ and 148‰. There is no obvious link to alteration or depth for these groupings.

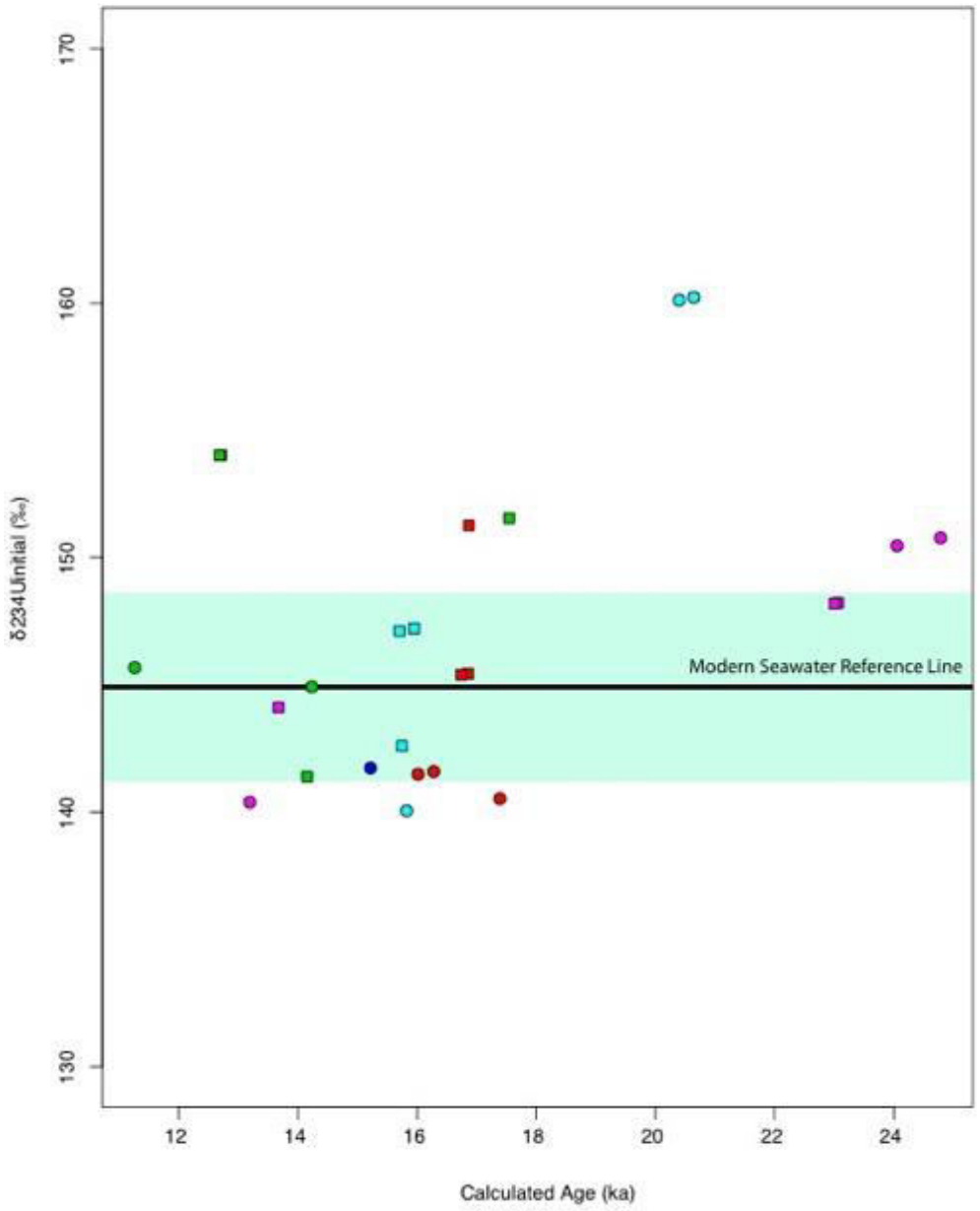

Figure 24. Calculated ages versus δ234initial with modern seawater δ234 (= 145‰) as a reference. The teal rectangle represents ±4‰, as a screening for problematic data analyses. δ234initial is back calculated using the measured δ234, the decay constant, and the calculated ages. There are seven samples, from all except Pristine category, that have δ234i that are higher than this range. This is one of the first signs that samples have been compromised. The three samples that are lower than this range could be explained by the changing of δ234sw throughout geologic history. Chutcharavan et al., 2018 argued that δ234sw has been variable during the last 20ka reaching as low as 143‰ at the time of the last deglacial. The abundance of lower δ234i found in this study helps support the lower δ234sw at this geologic time.

8.2.3 Closed System Screening

Prior to using PB U-Th age in any effort to reconstruct sea-level history, U-Th data must be carefully screened for any indication of open system behavior. Normally, U-Th data is screened for: (1) mineralogy, (2) δ234Ui (3) [232Th]. To continue with the trend of other published papers, we will screen these samples before interpreting them within the context of Penguin Bank and MWP-1a.

We screened our data using closed-system criteria based on prior publications (Hibbert et al., 2016; Scholz and Mangini, 2007). The mineralogy of our samples was determined using physical observations as well as EPMA point counts. The samples with high abundance of Mg-calcite cementation were noted, but not removed from the interpretations. Twelve of our dated samples had [U] within the average reported range of *Porites sp*. which is 2-4ppm (Hibbert et al., 2016).

Most cited studies use a cut-off of 2 pbb for [^{232}Th]. The issue with ^{232}Th is how much ^{230}Th it incorporates with it. However, we can calculate out detrital Th for our ages. Using initial Th values from Palmyra from Cobb et al. (2003) we can corrected our dates with a (^{230}Th/^{232}Th) of $4.4x10^{-6}$, which is the value for materials at secular equilibrium, assuming a bulk Earth crustal ^{232}Th/^{238}U ratio of 3.8. These corrections do not make any significant difference in our data and calculated ages. As well, our samples fall substantially below this concentration at ~2 ppb average.

An invaluable test of age reliability is a comparison of the measured and age corrected ^{234}U/^{238}U ratio to modern seawater (^{234}U/^{238}U = 1.145 or equivalently δ234Uinitial = 145‰) Hibbert et al., 2016; Sherman et al., 1999). This comparison is necessary but not alone sufficient

criteria for closed system behavior. Using the delta notation of this ratio $[((238-234)/238)*1000)]$, δ234Ui went through two steps for screening: 145±8‰ and 145±4‰. There are two samples that are higher of the first test (P5-844-17D =154‰ and P5-843-15C =160‰). Twelve of the samples fall within the second, more stringent test, ranging from 140.5‰ to 150‰.

There are three samples that do not fit these criteria that will not be used for interpretations. These samples are 841-17C, 841-17D, 843-15C. These samples have relatively low [U] (2.00 ppm, 1.96 ppm, 2.21 ppm, respectively) compared to the rest of the samples. These low [U] do not fit with the other data collected, i.e. [^{230}Th] and (^{234}U/^{238}U). This decrease in [U] could be because of an error in the laboratory or analyses. 843-15 samples have extremely high δ234Ui which do not make sense when interpreting the data against previous studies, analyses, and setting. Because these samples do not fit the screening criteria, they will not be used in the further interpretations of this study. Since one calculated age for 843-15 specimen is unreliable, the whole sample will not be used in interpreting changes due to alterations.

The 13 ages left fit the screening criteria and therefore they will be used in the interpretations. Nevertheless, these data are not free of their own problems. The dataset is small. The analytical uncertainties are larger than is typical, requiring cautious interpretation. The interpretations with this dataset can only be used so far. Further analyses, reruns, and data reduction on digestions of duplicate samples are needed to provide greater certainty to this dataset.

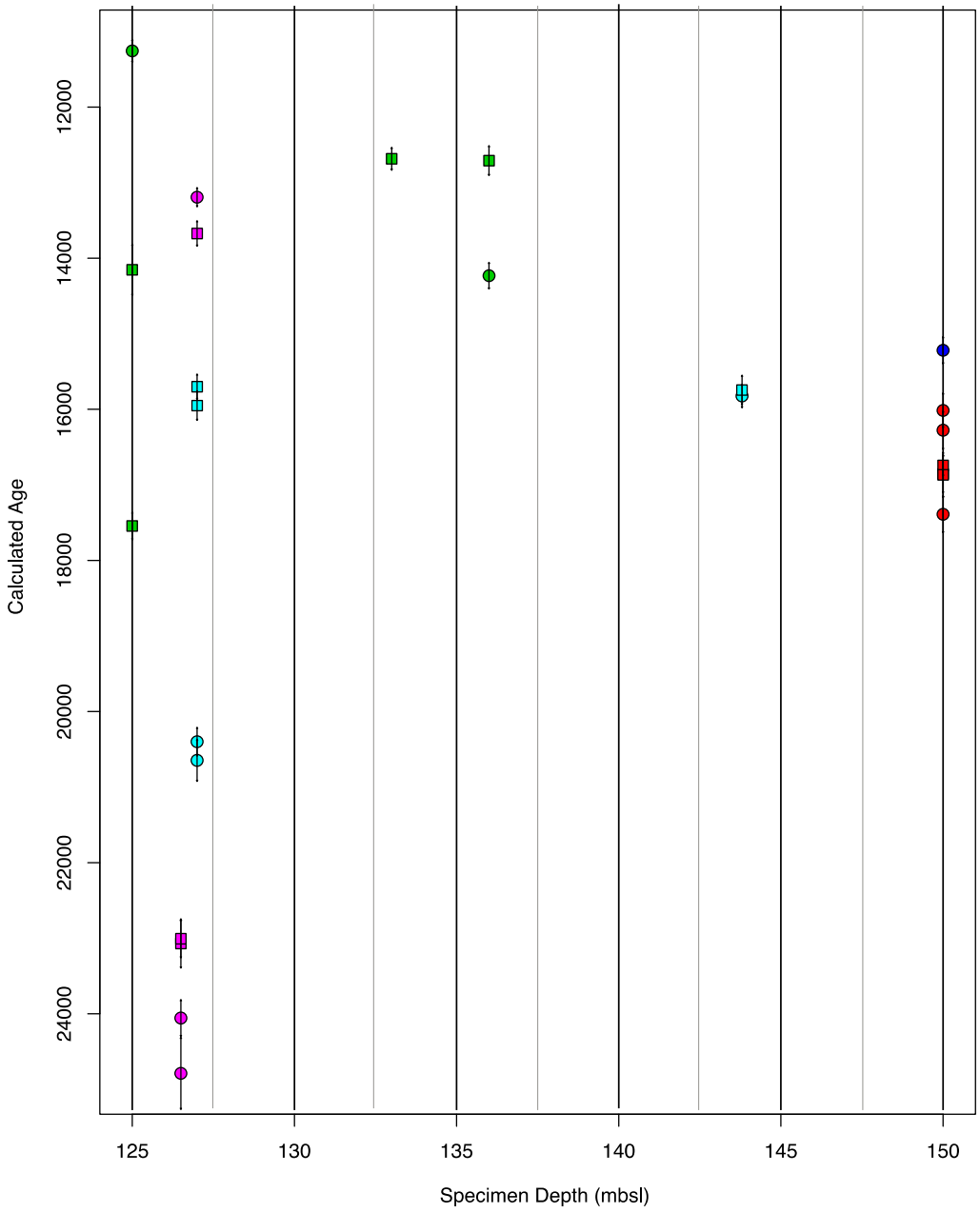

Figure 25. Specimen Depth (mbsl) vs. Calculated Age shows the range of ages in any given depth at Penguin Bank. This figure helps screen out compromised samples, such as the five lowest samples at about 126 mbsl. Physically and geologically there is no evidence that samples could have been growing over a span of almost 10,000 years at the same depth. The samples that are over 20ka old do not fit with the known sea level and depth ratio. The field relations and sample locations are inconsistent with a +20ka sample growing above 14-16ka samples . The rest of the samples fall within a depth/age ratio that has been previously observed at Penguin Bank

8.3 Major and Trace Element Analysis

Each alteration created physical changes in the samples, but there is no discernable change chemically. By comparing analyses taken along the alteration contact, transect through the alteration to pristine areas, and just in pristine areas, we are able to determine any elemental changes due to alteration (Table 6).

Alkaline Earth Element Composition

Type of Sample	Sample Name	CaO	±	MgO	±	SrO	±	Mg/Ca	±	Sr/Ca	±
Pristine	750-07	54.75	0.05	0.15	0.01	0.90	0.01	3.89	0.08	8.89	0.08
Discoloration	750-11	52.81	1.36	0.14	0.01	0.81	0.04	4.38	0.33	7.11	0.24
	284-13	54.11	0.27	0.15	0.01	0.92	0.02	4.62	0.22	7.94	0.20
Coralline Algae Overgrowth	841-17	54.74	0.13	0.14	0.01	0.91	0.02	4.20	0.24	7.74	0.19
	841-11	55.08	0.22	0.15	0.01	0.89	0.03	4.49	0.38	7.49	0.23
Bioerosion	841-07	55.00	0.02	0.13	0.01	0.90	0.01	3.84	0.05	7.66	0.02
	843-15	54.58	0.01	0.14	0.01	0.86	0.01	4.38	0.01	7.37	0.01
Sponge Ingrowth	749-08	54.53	0.10	0.13	0.01	0.90	0.01	4.13	0.08	7.67	0.08
	844-17	54.02	0.12	0.18	0.01	0.86	0.04	5.54	0.32	7.42	0.32

Table 6. Bulk by average coral skeleton for each samples separated into alteration category. The measured elements reflect an assumed aragonite skeleton. Average overall coral skeleton mineralogy for each sample. Mg/Ca and Sr/Ca are within average reported values. (Lazar et al., 2004, MacIntrye, 1997). Oxides are in wt%; ratios in mmol/mol; 2σ standard error reported (n=503).

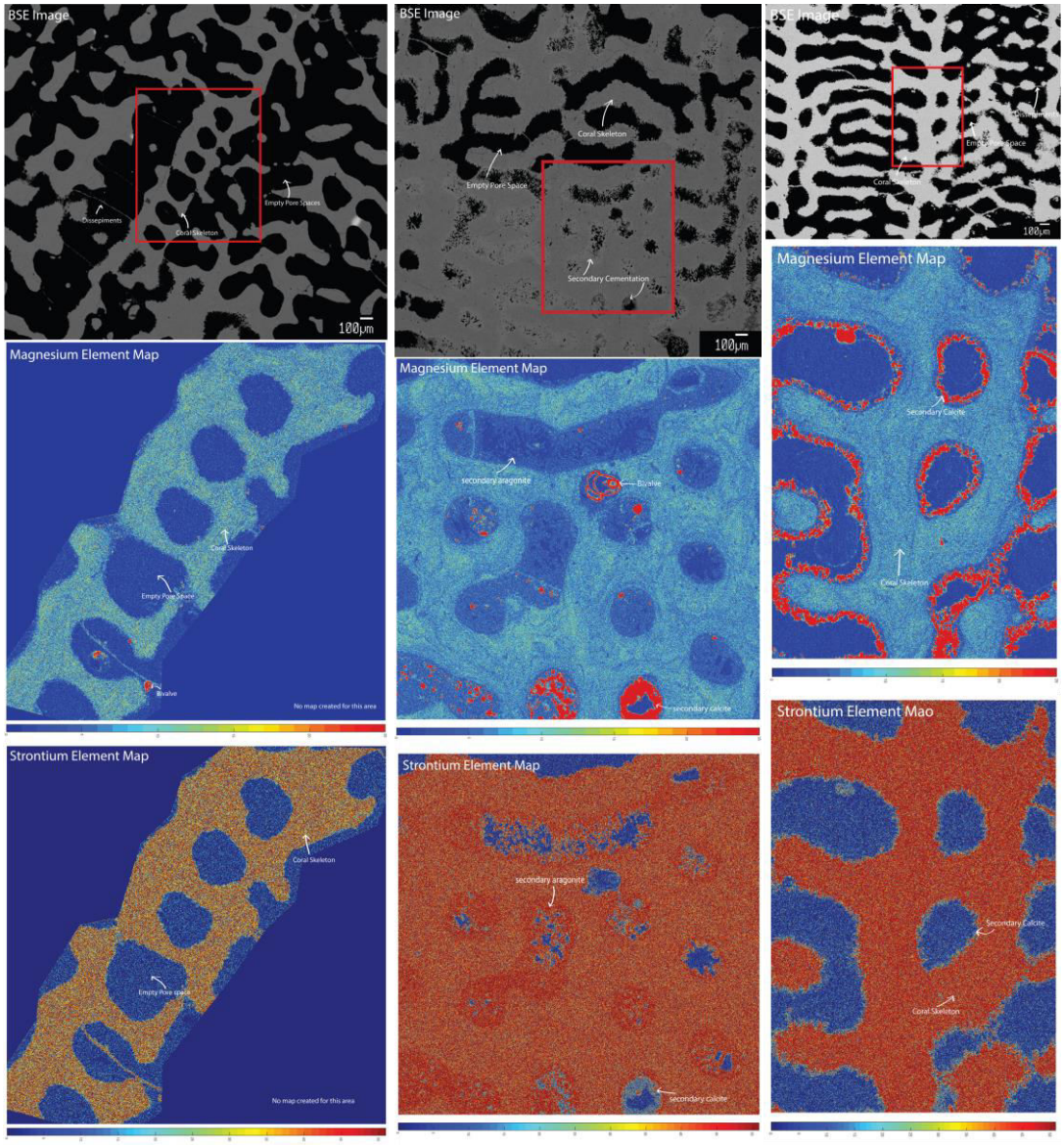

Figure 26. EMPA element maps for Sr and Mg to show relative concentrations in parts of specimen. (Left) Element map of pristine primary aragonite skeleton. Compositionally homogeneous with an average of 54wt% CaO, 0.15wt%MgO, and 0.9 wt% SrO. Annotations show primary aragonite skeleton and empty pore space. Top image: BSE image, red box where distribution map was taken. Middle Image: Qualitative magnesium distribution map; Bottom Image: Qualitative strontium distribution map. The two different distribution maps are not at the same scale. (Middle) Primary aragonite skeleton overgrown with first-generation acicular aragonite cement as well as some Mg-calcite cement. Top image: BSE image, red box is distribution map. Middle Image: qualitative magnesium distribution map. Shows the depletion of Mg in aragonite cement, as well as the enrichment of Mg in Mg-calcite cement. A bivalve within a pore can be seen within the map. Bottom Image: qualitative strontium map showing the enrichment of Sr within aragonite cement. The two different distribution maps are not at the same scale. (Right) Primary aragonite skeleton overgrown with first-generation Mg-Calcite cement. Top Image: BSE image, red box is mapped area. Middle Image: qualitative magnesium distribution map showing the enrichment of Mg in the calcite cement. The isopachous, bladed spar morphology is well-seen in this map. Bottom Image: qualitative strontium distribution map showing the depletion of Sr within calcite cement.The two different distribution maps are not at the same scale

The “pristine” corals have mostly intact, well-formed skeletons (Figure 17). There are a few fractured parts where there is aragonite cementation. Otherwise, these samples show no other forms of disturbance or alteration. On average, the elemental make-up of these pristine samples is 54.9±1.33 wt% CaO, 0.15±0.066 wt% MgO, and 0.90 ±0.23wt% SrO (n=112). The Mg/Ca and Sr/Ca are 4.70±1.02 mmol/mol and 7.65±0.99 mmol/mol, respectively. Pristine samples were used to represent the natural variation within the corals. Compared to the one categorically Pristine sample measured, all “pristine” sections of the categorically altered specimens are either within error or the same value. Statistically the “pristine” section of an altered coral is the same as a completely pristine coral.

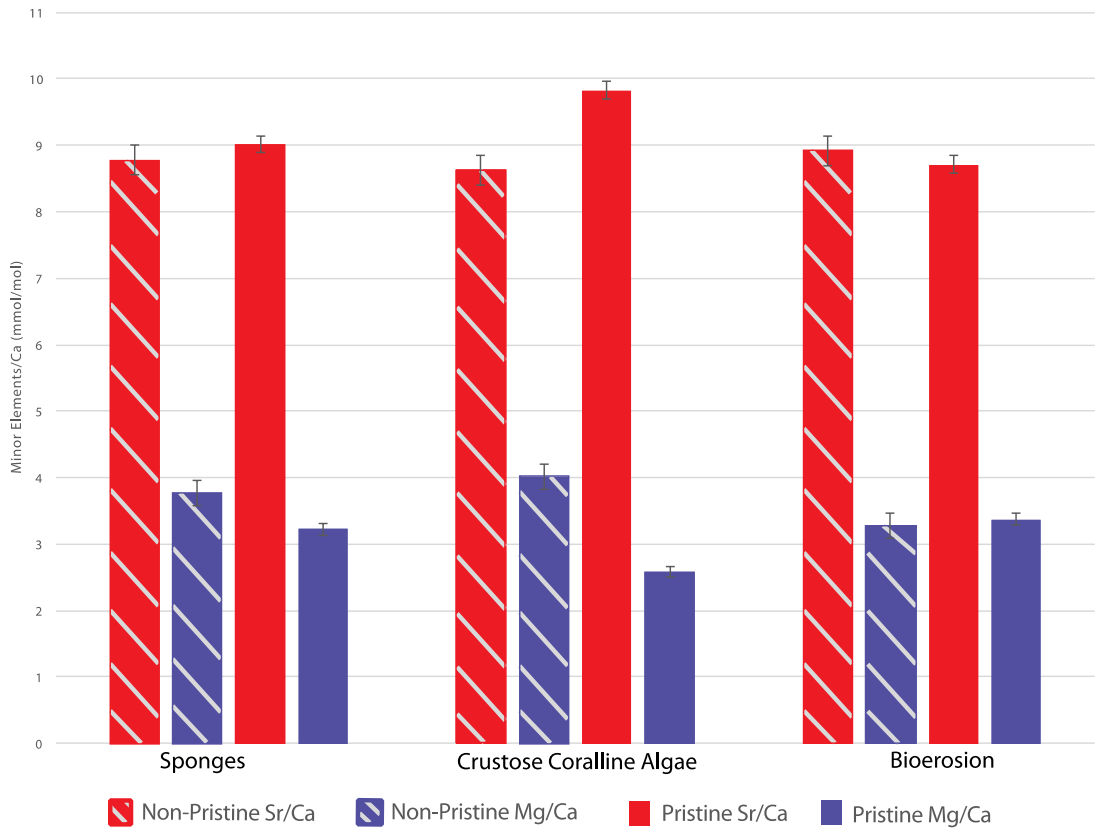

Figure 27. Graph showing Sr/Ca and Mg/Ca ratios of altered vs. unaltered sections of samples. Coralline Algae is the only alteration that shows significant change between the two sections. The altered section has substantially more Mg/Ca within the primary aragonite. Error bars are 2σ

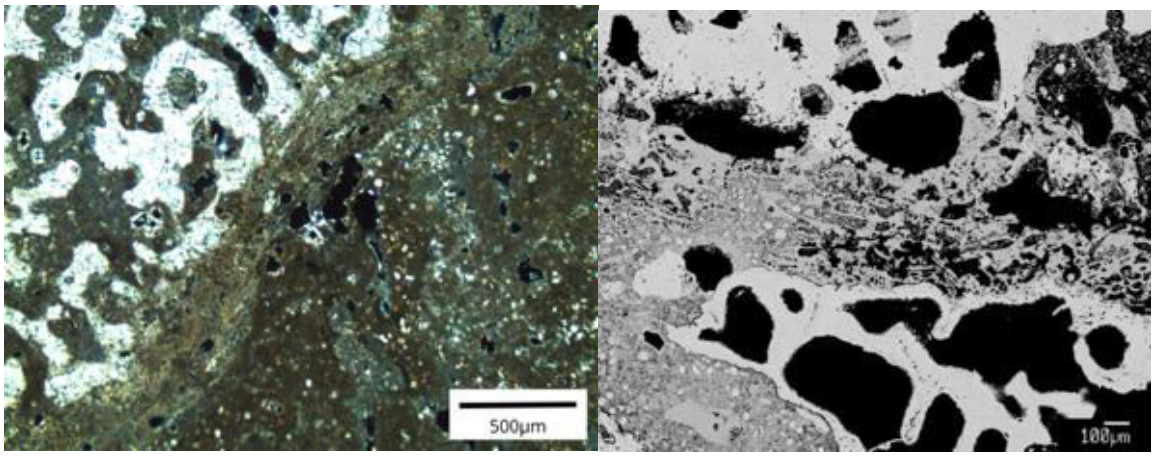

Figure 28. Coralline Algae growth over coral skeleton. Left: Optical Microscope image (PPL) of coralline alge overgrown on coral skeleton. Coral pores are completely filled by Mg-Calcite cement. The layer in the center of the image is coralline algae covered by a carbonate crust made of similar material to the Mg-Calcite cement. Right: BSE image of a similar coralline algae overgrowth.

Crustose coralline algae (CCA) are non-geniculate, red algae of the order *Corallinales* that secrete Mg-calcite skeletons. It is disputed whether CCA helps or hinders the growth of reefs. Most specimens from Penguin Bank have some sort of CCA overgrowth. In this study, specimens with coralline algae overgrowth were much more likely to have pores filled with Mg-calcite cement. The amount of Mg-calcite increases closer to the alteration contact. The coral skeleton along the edges of the contact have a composition of 54.6±1.5 wt% CaO, 0.10±0.08 wt% MgO, and 0.99±0.26 wt% SrO (n=76. The Mg/Ca and Sr/Ca are 2.58±0.9 and 9.82±1.19 mmol/mol, respectively. The un-altered skeleton, at least 2mm away from the coralline algae, has Mg/Ca and Sr/Ca ratios of 3.27±0.63 and 8.9±0.44 mmol/mol and an overall composition of 54.9±0.60 wt% CaO, 0.12±0.04 wt% MgO, and 0.90±0.08wt% SrO (n=25). As seen in Table 5 and Figure 16 and 18, the coral skeleton near the coralline algae is slightly enriched in Mg/Ca.

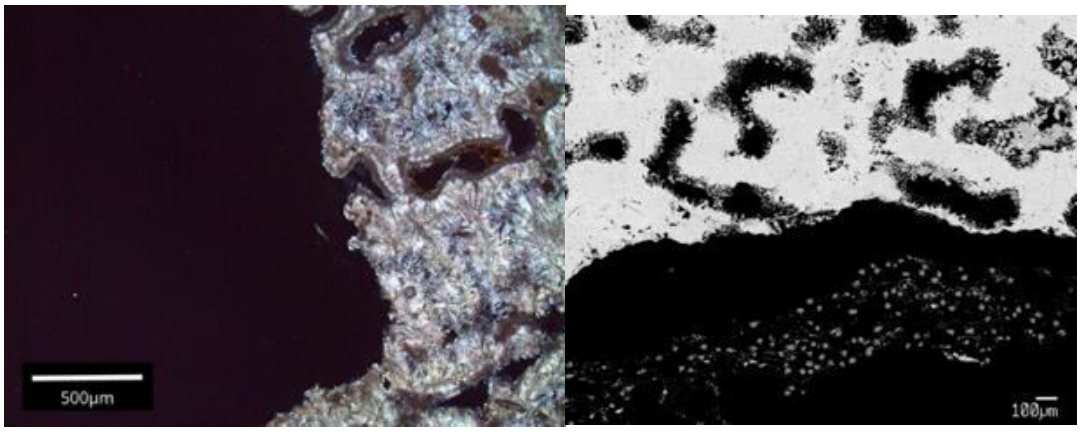

Figure 29. Edge of Bioerosion. Left: Optical Microscope image (XPL) showing the edge of a borehole. Both marine cements are visible. Aragonite cement forms the acicular needs and the Mg-calcite forms isopachous and optically darker rims along the pores. Right: BSE image of a similar bioeroded area with organic material within the borehole. Both marine cements are also seen.

Bioerosion occurs when an organism (endolith) that has either physically removed or chemically dissolved the coral skeleton. There are many different species of borers: some which bore when the coral is alive and some which bore after the coral has died. Studies have shown that the rate of bioerosion does not vary much between living coral and dead coral Le Campion-Alsumard et al., 1995; Tribollet, 2008). Bioerosion is characterized by clean, sharp edges as well as residual organic material. Any mechanical changes would only physically disturb the coral. Chemical dissolution could possibly affect the coral skeleton composition. In this study, we found that the amount of cementation, especially Mg-calcite, increases closer to the bioerosion (Figure 19). The altered sections of the coral skeleton (near borehole edge) have an average composition of 54.73±1.12 wt% CaO, 0.13±0.052 wt% MgO, and 0.88±0.16 wt% SrO (n=207). The Mg/Ca and Sr/Ca averages are 3.37±0.68 and 8.71±0.84 mmol/mol, respectively. The coral skeleton not affected by bioerosion has a composition very near to the composition of totally pristine specimens.

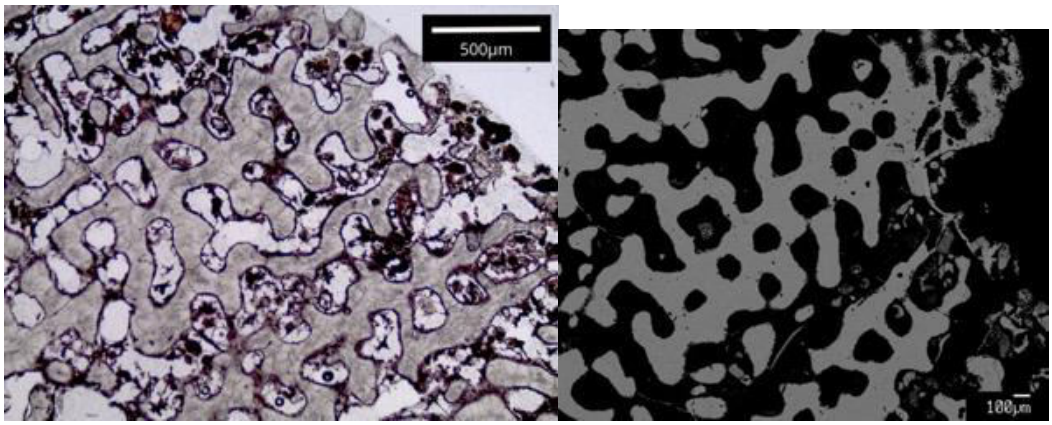

Figure 30. Left: Optical Microscope image of Sponge within coral skeleton (PPL). The sponge has grown within the coral skeleton pores, leaving a purple stain on the coral. Right: The same portion of coral skeleton in Backscattered Electron. The sponge is not observable in the BSE image.

Sponges are another vital part of a reef system. They grow with and around the corals. The most common types found on Penguin Bank specimens are crustose, organic sponges that grow either on top of or inside the coral. This study examined a single occurrence on each type of sponge growth. The specimen with the sponge inside the coral skeleton shows almost no compositional or physical change (Figure 20). The specimen with the sponge growth on top shows some secondary cementation. The sponge physically removed some of the coral as indicated by broken aragonite pieces within pores around the sponge. This most likely happened while the sponge was attaching itself to the coral. The composition of the un-altered skeleton is 54.9±1.13 wt% CaO, 0.15±0.06 wt% MgO, and 0.87±0.20 wt% SrO. The average Mg/Ca is 3.22±0.08 mmol/mol (n=74). The average Sr/Ca is 9.01±0.13 mmol/mol with a range of 6.44 to 10.37. The altered skeleton is 54.63±1.0 wt% CaO, 0.13±0.05 wt% MgO, and 0.91±0.23 wt% SrO (n=23). The skeleton altered by the sponge has an average Mg/Ca of 3.76±0.19 mmol/mol and Sr/Ca of 8.77±0.22 mmol/mol.

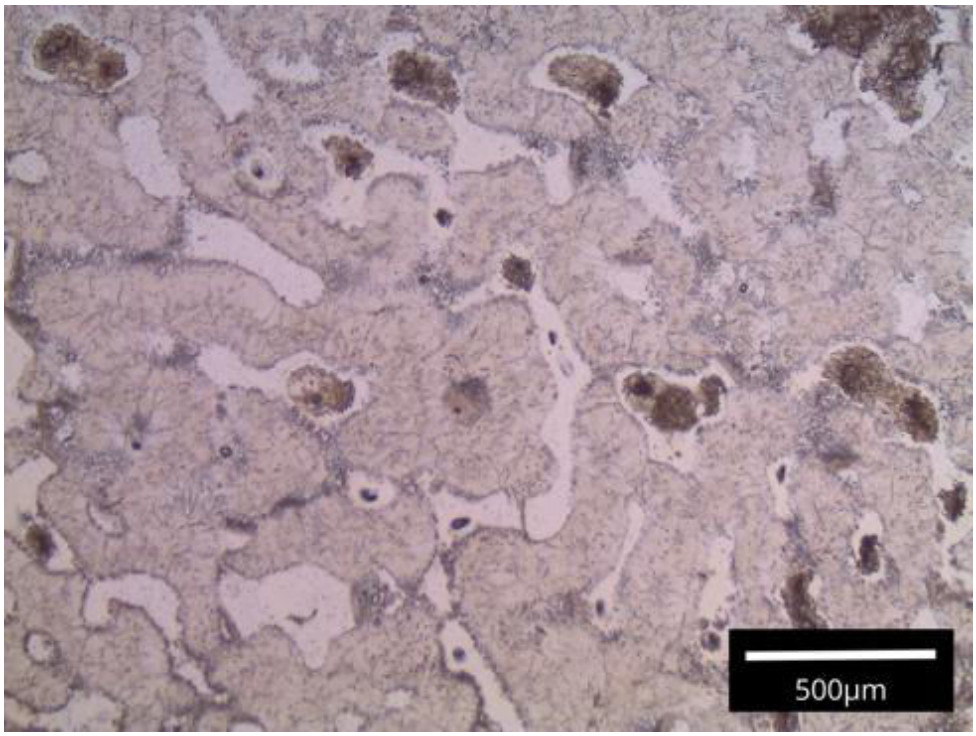

Figure 31. Plain Light Optical Microscope image of detrital material within pores of coral skeleton.

Discoloration in hand sample is attributed to detrital material within the pores. Depending on the timing, this material could leach into porewater, allowing for changes in the composition of the cementation (Esat and Yokoyama, 2006). However, the discoloration is difficult to see under the microscope (Figure 21) and the electron probe. It is difficult with BSE images to determine where the sample is discolored. The whole sample could be considered altered. The coral skeleton average for samples with discoloration is 54.34±1.06 wt% CaO, 0.15±0.06 wt% MgO, and 0.94±0.26 wt% SrO (n=35) . The Sr/Ca and Mg/Ca are 9.36±1.27 and 3.88±0.79 mmol/mol, respectively.

Most Sr/Ca and Mg/Ca ratios fall within the natural range calculated from our two pristine samples (Table 5). There is no measureable difference between the altered and unaltered sections for corals with boreholes and/or ingrown sponges. A slight increase in Sr and decrease

in Mg can be seen in the coral near coralline algae overgrowth, possibly indicating an increase in U in this area. However, for all other areas, we are unable to detect these differences and infer U-Th effects at this resolution. Distribution maps (Figure 26) show us a distinguishable difference between the coral skeleton and the secondary cements present. Sr is homogeneous throughout both coral skeleton and secondary aragonite at this resolution. Mg shows heterogeneity which could be consistent with growth patterns.

9. Interpretations

9.1 Alterations

In order to understand the changes we see in U-Th data, we have to compare the data to the known timings of MWP-1a. In this section, we will discuss each specimen pair (pristine and non-pristine), the variations displayed, and what may have caused them. For Crustose Coralline Algae and Bioerosion, we only have one specimen to use for interpretations. For Sponges and Discoloration categories, we have two specimens. Our interpretations will be limited because of this. Up until this point we have assumed a closed system to calculate these dates, but in order to explain the variations, we need to assume some open system behavior.

9.1.1 Coralline Algae Growth

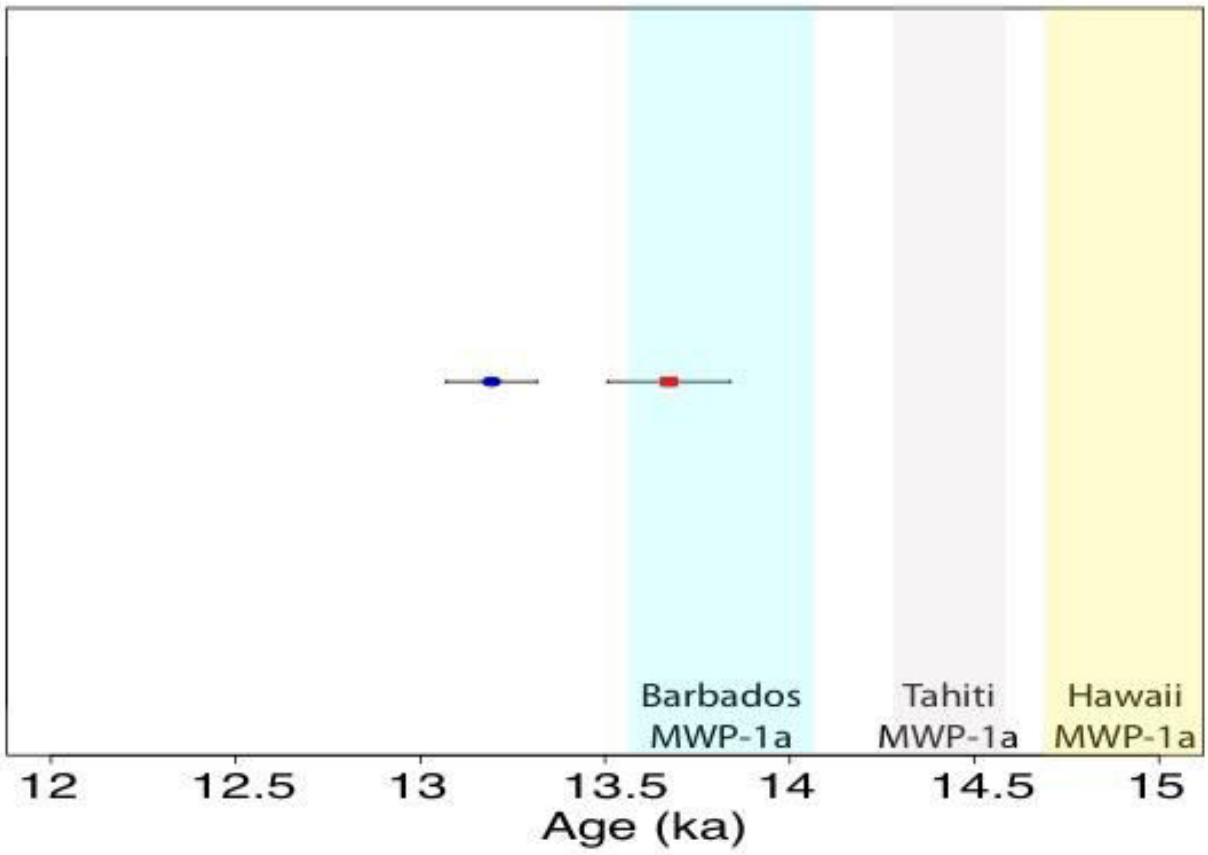

Figure 32. Specimen 841-11 with overgrowth of Crustose Coralline Algae. Pristine sample (blue circle) calculated date is compared to non-pristine sample (red square) calculated date. To give context, the timings of MWP-1a for Barbados (teal; 14.08-13.61ka), Tahiti (grey; 14.65-14.3ka), and Hawai'i (yellow; 15.2-14.7ka) are shown.

For specimens with Crustose Coralline Algae, there is only one reliable specimen. As seen in figure 32, the samples span about 100 years at the highest error. This is almost half of the timing of MWP-1a at Tahiti. There is a large variation in physical make-up of the samples, having one of the higher percentages of secondary calcite. Uranium preferentially goes into aragonite. Calcite has a much lower concentration of uranium (Lachniet et al.,2012). As seen in our measurements, the pristine sample has a [U]=3.71 ppm, whereas the non-pristine sample has a [U] = 2.91 ppm. The extra presence of secondary calcite could make the [U] lower. Having a

lower [U] will generate an older calculated date, although a shift of this magnitude implies nearly 25% calcite addition, which is visually not observed.

9.1.2 Sponges

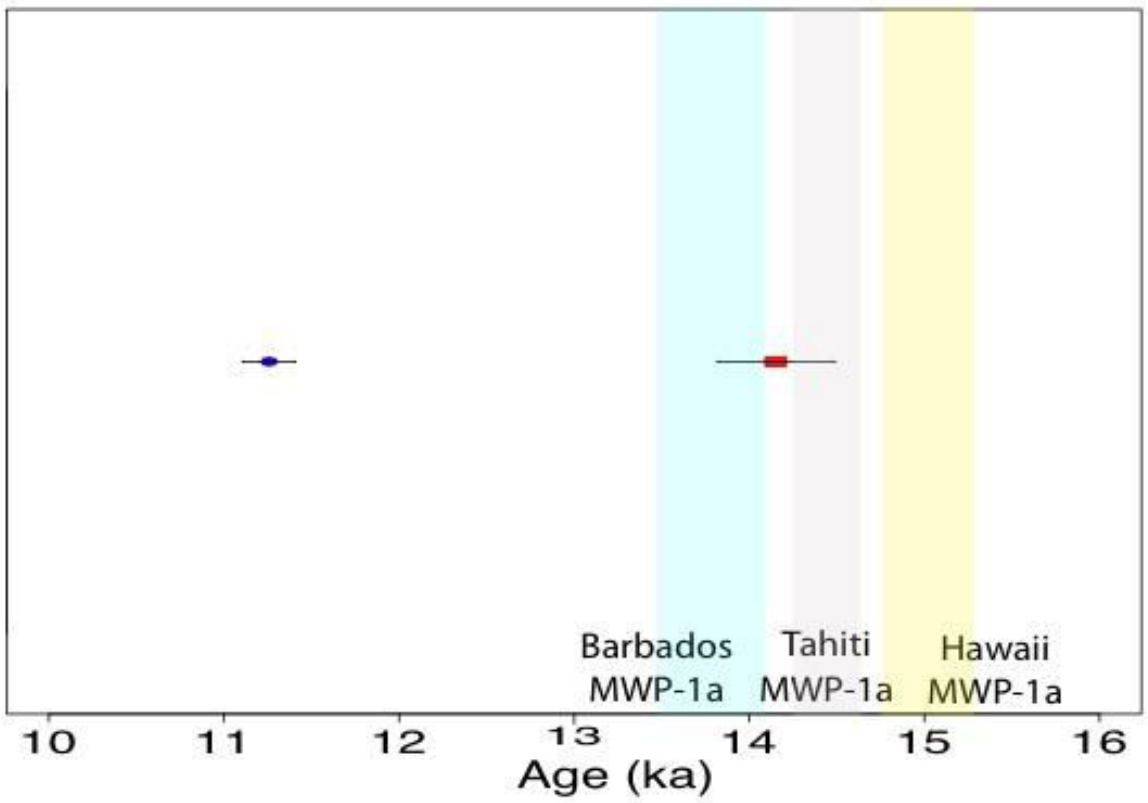

Figure 33. Specimen 749-08 with ingrown sponge. Pristine sample (blue circle) calculated date is compared to non-pristine sample (red square) calculated date. To give context, the timings of MWP-1a for Barbados (teal; 14.08-13.61ka), Tahiti (grey; 14.65-14.3ka), and Hawai‘i (yellow; 15.2-14.7ka) are shown.

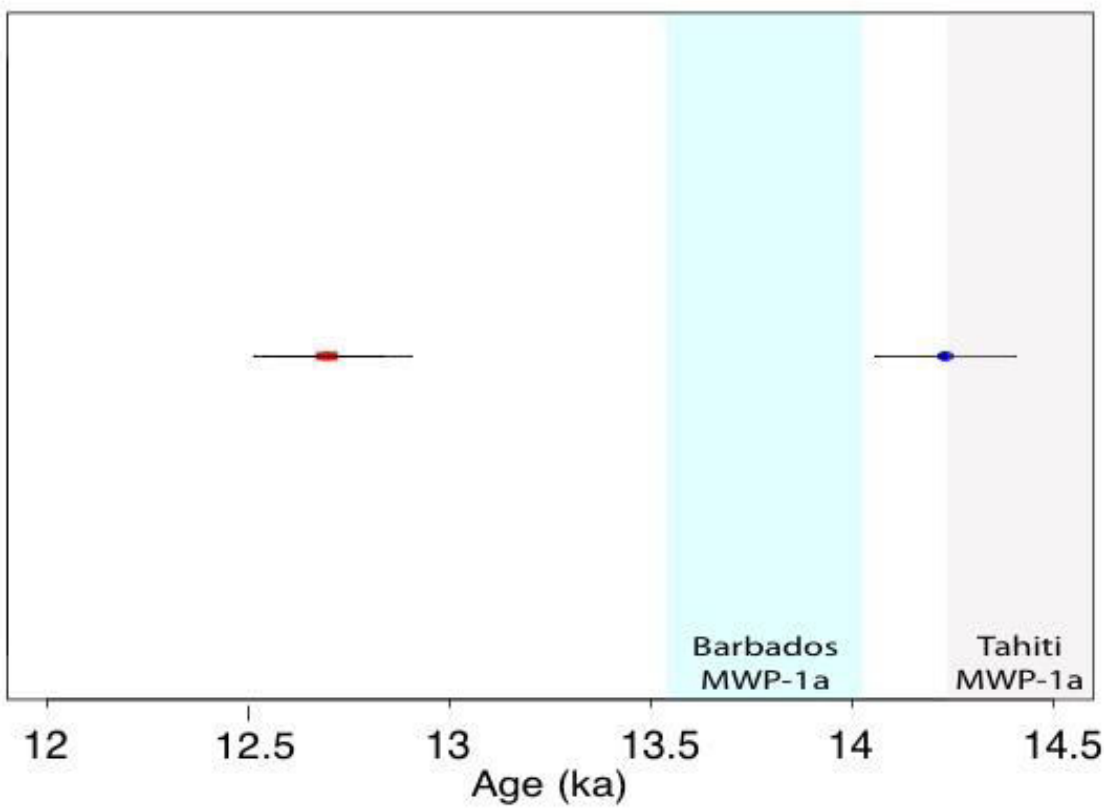

Figure 34. Specimen 844-17 with ingrown sponge. Pristine sample (blue circle) calculated date is compared to non-pristine sample (red square) calculated date. To give context, the timings of MWP-1a for Barbados (teal; 14.08-13.61ka), Tahiti (grey; 14.65-14.3ka), and Hawai‘i (yellow; 15.2-14.7ka) are shown. Only Barbados and Tahiti are shown because the sample is too young to compare to Hawai‘i timing.

There are two reliable specimens for sponge alterations. For specimen 844-17 (Figure 33), the pristine sample is much younger than the non-pristine sample. However, the exact opposite happened for specimen 749-08 (Figure 34). Both specimens show large variations between pristine and non-pristine sections. We are not able to form a full hypothesis for the process that sponges change U-Th, but they do strongly affect the precision of dating. Thankfully, sponges are easy to identify and avoid during sampling.

9.1.3 Bioerosion

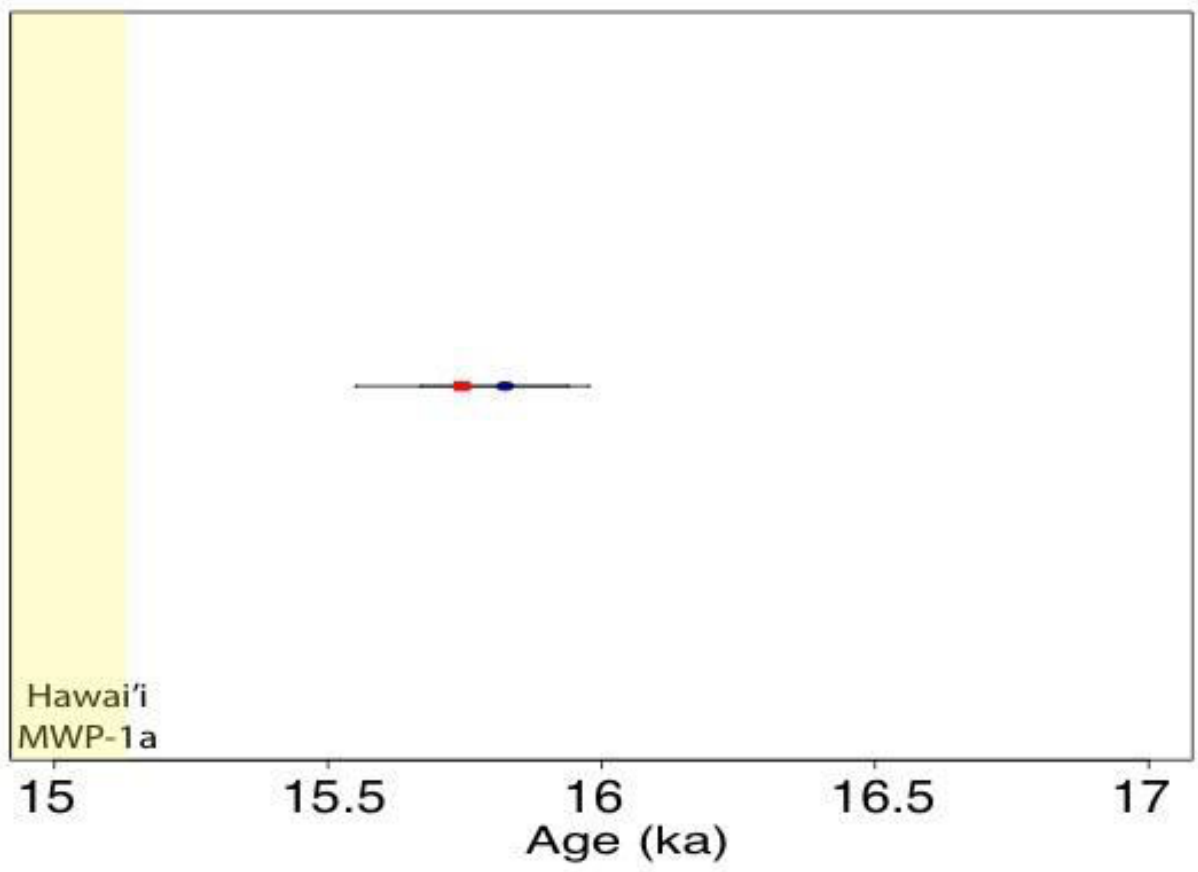

Figure 35. Specimen 841-07 with bioerosion Pristine sample (blue circle) calculated date is compared to non-pristine sample (red square) calculated date. To give context, the timings of MWP-1a for Barbados (teal; 14.08-13.61ka), Tahiti (grey; 14.65-14.3ka), and Hawai'i (yellow; 15.2-14.7ka) are shown. Only Hawai'i is shown, because the sample is too old to see Tahiti and Barbados timings.

There is only one reliable sample for bioerosion. Specimen 841-07 (Figure 35) shows no substantial change between the pristine and non-pristine, because the samples are within error. This specimen has the largest amount of secondary aragonite. Lazar et al. (2004) has shown that an increase in secondary aragonite has been shown to increase U concentration. The pristine sample has [U] = 3.07 ppm. The non-pristine sample has a [U] of 3.30 ppm. This increase in secondary aragonite, and therefore [U], in the non-pristine sample makes the age calculated younger.

4.1.4 Discoloration

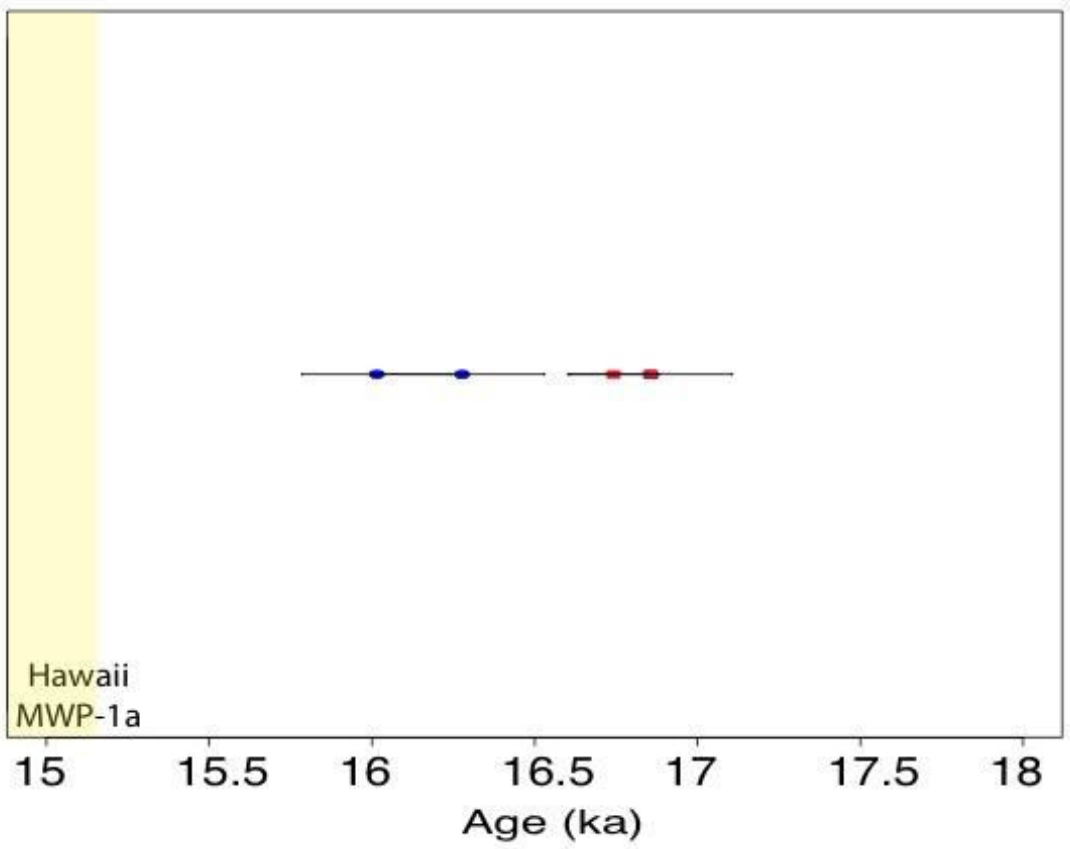

Figure 36. Specimen 750-11 with discoloration. Pristine sample (blue circle) calculated date is compared to non-pristine sample (red square) calculated date. To give context, the timings of MWP-1a for Barbados (teal; 14.08-13.61ka), Tahiti (grey; 14.65-14.3ka), and Hawai‘i (yellow; 15.2-14.7ka) are shown. Only Hawai‘i is shown, because the sample is too old to see Tahiti and Barbados timings.

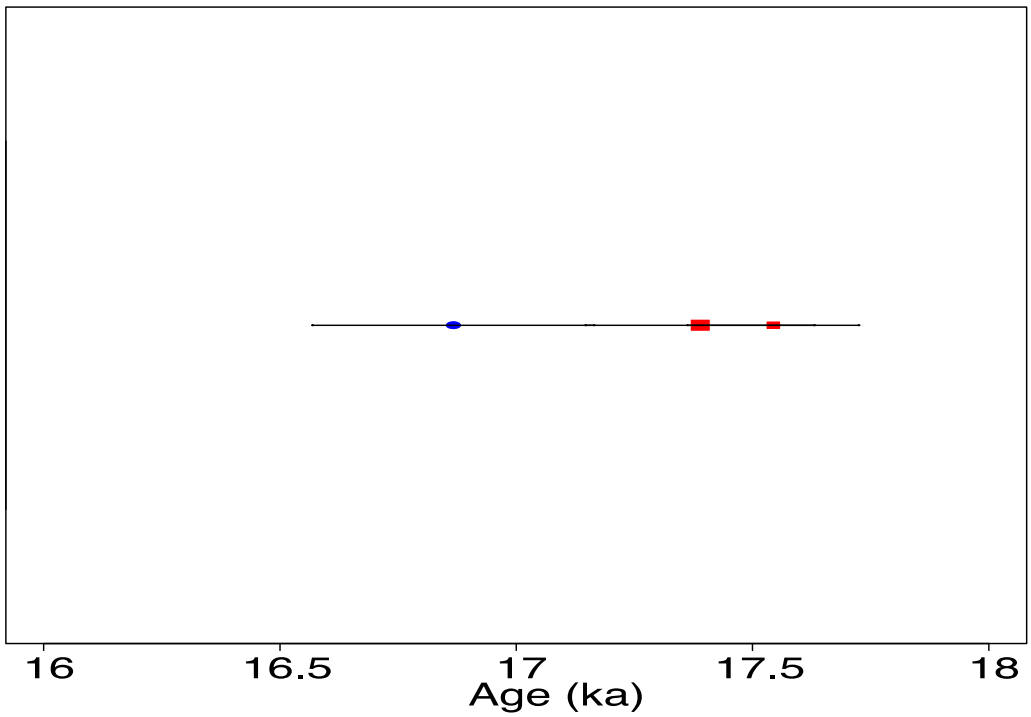

Figure 37. Specimen 284-13 with discoloration. Pristine sample (blue circle) calculated date is compared to non-pristine sample (red square) calculated date. To give context, the timings of MWP-1a for Barbados (teal; 14.08-13.61ka), Tahiti (grey; 14.65-14.3ka), and Hawai‘i (yellow; 15.2-14.7ka) are shown. No bars are present, because the sample is older than the three separate timings.

Both specimens for discoloration are reliable, and the pristine and non-pristine samples are either within error or less than 50 yrs apart (Figure 36 and 37). The variation between the two sections is the smallest in these specimen, showing that discoloration does not have that large of an effect on the precision of dating. Both specimens are older than the known timing for MWP-1a, but that is because they are from a depth of 160m, making them some of the oldest specimens at Penguin Bank.

9.1.5 Overall

In spite of the complex nature of the data and the relatively large analytical uncertainties, it is clear that mesophotic alteration of these corals has produced some small but detectable disturbances in the uranium thorium systematics. The mechanisms of alterations to U-Th data are not fully understood with this small, exploratory data set. Much more work is needed.

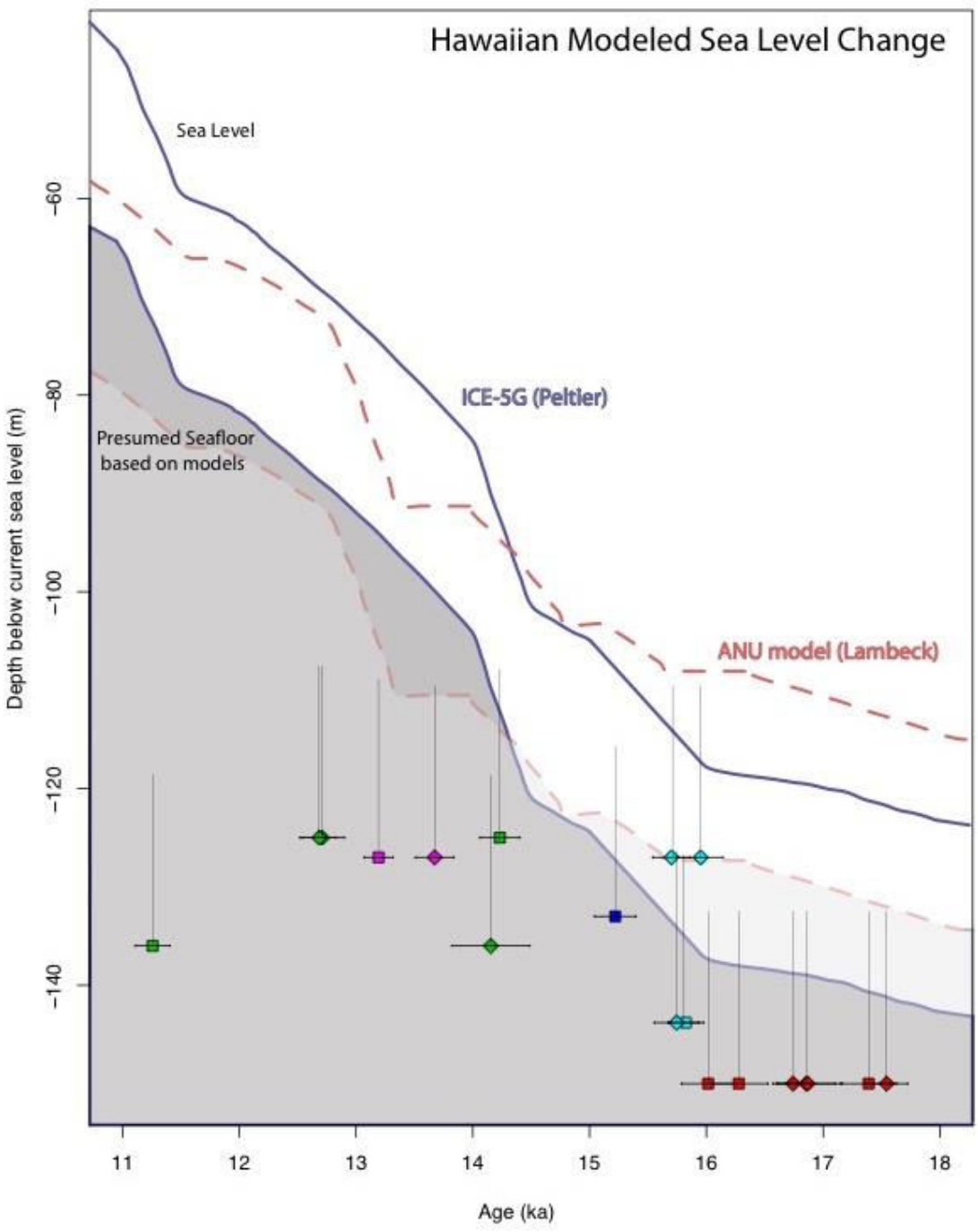

Figure 38. Reliable Specimens plotted Age vs Depth displays the correlation with age and depth as well as rising sea level. The youngest ages also being the shallowest.. Squares are non-pristine. Diamonds are pristine samples. Alteration categories are Crustose Corraline Algae (teal), Bioerosion (pink), Sponge (Green), Discoloration (Red), Pristine (Blue). The calculated ages are also plotted with two different Hawai'ian deglacial sea level models (Lambeck, dashed red; Peltier, solid purple). Probable relative sea level (~20 mbsl) created from Monte Carlo simulation based on median Porites sp. depth (5-40 mbsl) range are vertical grey lines on data points (Based on calculations by Hibbert et al., 2016).

9.2 Penguin Bank

Our calculated ages fit with the depth/age relationship seen in already dated Penguin Bank corals (Rubin, unpublished). The older specimens (around 16-17ka) are found around 160 mbsl. As the depth decreases, the specimen ages become younger. When compared to Hawaiian deglacial sea level models (Lambeck et al. 2014; Peltier et al., 2002), the specimens follow the trend of slowly rising sea level until MWP-1a. At around 14 ka, or the onset of MWP-1a, we stop seeing a depth/age trend. Figure 38 shows that the specimens start to grow at deeper depths than previously. At this depth today, we see 10m high coral mounds. During the rapid rise in sea level, the corals at Penguin Bank kept up with sea level by creating these mound structures. The fact that we do not see this quick growth in this dataset could be from sampling bias due to only selecting samples from the bottom of these mounds. The change in depth/age relationship could also be due to the excellent ocean environment, which allowed the corals to grow at the deeper end of their depth range. Lastly, sea level could have outpaced the coral growth rate, and the corals "caught up" to the sea level after the MWP, and we do not have the specimen to show this.

9.3 MWP-1a

Meltwater Pulse 1a magnitude and timing around the globe is shown in Figure 40. The ages from Penguin Bank are plotted with other MWP-1a data. There is a large offset between PB and the other datasets. This could be caused by (1) no cessation of growth due to rapid sea level rise at Penguin Bank, (2) the GIA models being used are different, (3) tectonic subsidence or uplift corrections are incorrect for other areas. We are not yet able to refine the timing of MWP-1a any more with this dataset.

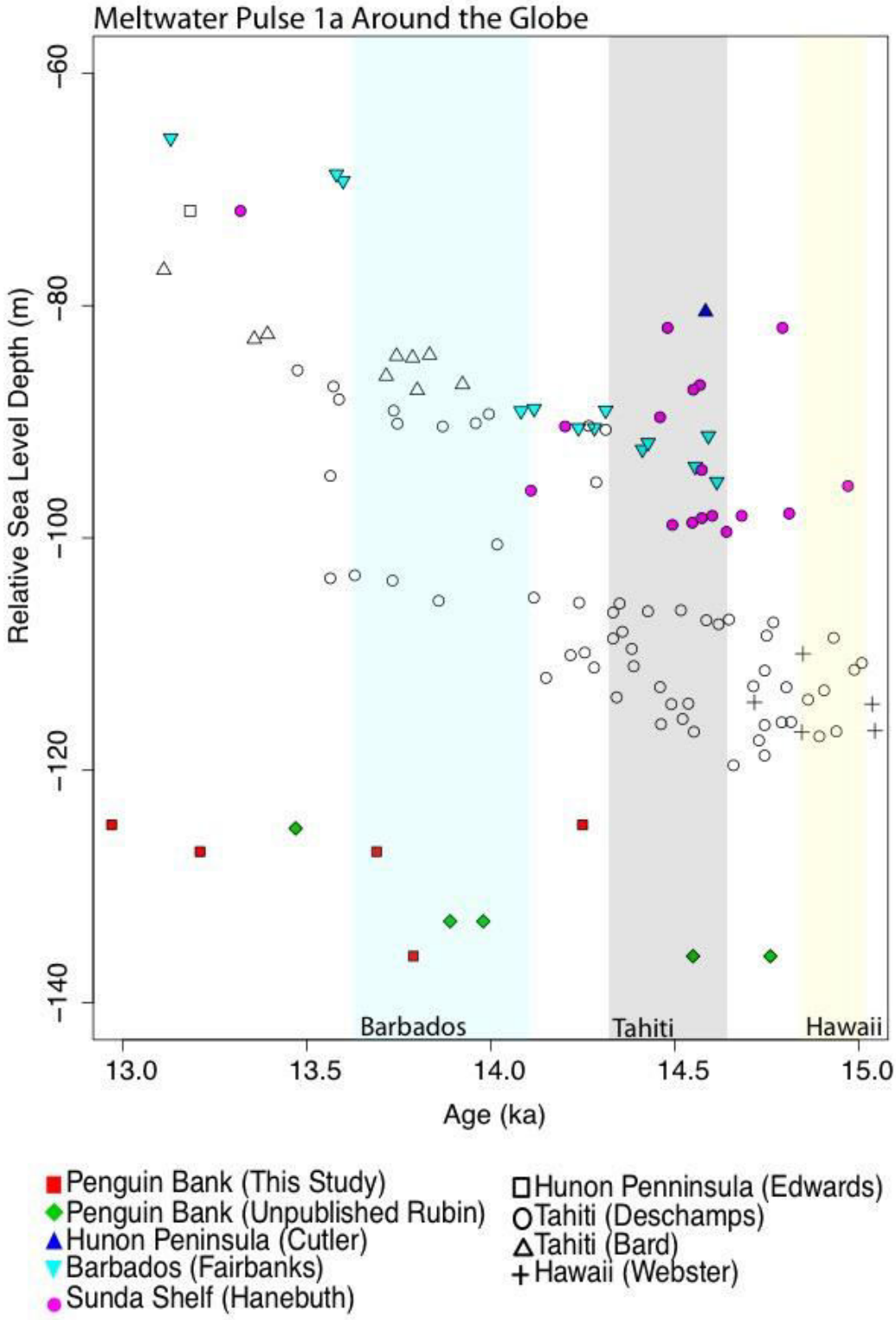
Meltwater Pulse 1a Around the Globe
Relative Sea Level Depth (m)
−60
−80
−100
−120
−140
Barbados
Tahiti
Hawaii
13.0
13.5
14.0
14.5
15.0
Age (ka)
Penguin Bank (This Study)
Penguin Bank (Unpublished Rubin)
Hunon Peninsula (Cutler)
Barbados (Fairbanks)
Sunda Shelf (Hanebuth)
Hunon Penninsula (Edwards)
Tahiti (Deschamps)
Tahiti (Bard)
Hawaii (Webster)

Figure 39. Figure edited from Sandborn, 2017 with new Penguin Bank data (red squares, this study and green diamond, unpublished Rubin). Plotted are global sea-level records, including Tahiti (unfilled triangles, Bard et al, 2010 and circles, Deschamps et al., 2012), Barbados (teal upside down triangle, Fairbanks et al, 2005 and Peltier and Fairbanks, 2006), Hunon Peninsula, Paupa New Guinea (blue triangle, Edwards et al., 1993; unfilled square, Cutler et al, 2003), and Sunda Shelf (pink circles, Hanebuth et al, 200). The vertical bands indicate timing of MWP-1a based on the Tahiti (grey band, 14.65-14.3ka; Deschamps et al.,2012, Camoin et al., 2012), Barbados (teal band, 14.08-13.61ka, Fairbanks, 1989), and Hawai‘i (yellow band, 15.2-14.7ka, Webster et al., 2004). Error Bars are not shown in this figure.

10. Conclusions

This study aimed to understand what variations could be seen in U-Th disequilibrium systematics for corals subject to long-term colonization/alteration within the mesophotic zone. By picking a range of samples from a known depth and an assumed age, we were able to see the effects of mesophotic alterations. We approached this problem in two steps: (1) observing physical and minor element changes to the coral skeleton using electron probe microanalysis and (2) creating a suite of U-Th isotope data to calculate ages and compare pristine and non-pristine samples.

We measured on average CaO concentration of 54 wt%, MgO of 0.15 wt%, and SrO of 0.9 wt%. Mg/Ca, on average, was 3-4 mmol/mol, and Sr/Ca was 9-10 mmol/mol. We were not able to determine changes within the coral skeleton at the resolution used by the electron microprobe.

Using measurements of [^{238}U], [^{230}Th], (^{234}U/^{238}U), we were able to measure and calculate 13 reliable ages for Penguin Bank corals. Four samples were not reliable based upon evaluation of the initial uranium isotope ratio and the geologic variability of the calculated ages. The rest of the samples show that there are some changes due to the mesophotic alterations present on the specimens. There is no overarching pattern. Each alteration category changes the data and, therefore, the ages in a different way. However, since the dataset is small and there are problems with it, the we cannot make any supported conclusions about what and how these alterations change the specimens and our abilities to accurately date them.

It would be premature to recommend any procedural changes in thorium uranium dating methods based on the study. The most robust conclusion is that the effects of long-term mesophotic alteration of corals does impact U-Th ages. We recommend the continual use of screening methods of visual and microscopic observations to pick out the most pristine sections of coral to date sea level events.

11. References

Abdul, N. A., Mortlock, R. A., Wright, J. D., & Fairbanks, R. G. (2016). Younger Dryas Sea-Level and Meltwater Pulse 1B Recorded in Barbados Reef-Crest Coral Acropora palmata. *Paleoceanography*, n/a-n/a. https://doi.org/10.1002/2015PA002847.Received

Allison, N. (1996). Geochemical anomalies in coral skeletons and their possible implications for palaeoenvironmental analyses. *Marine Chemistry*, *55*(3–4), 367–379. https://doi.org/10.1016/S0304-4203(96)00060-6

Allison, N., Finch, A. A., Webster, J. M., & Clague, D. A. (2007). Palaeoenvironmental records from fossil corals: The effects of submarine diagenesis on temperature and climate estimates. *Geochimica et Cosmochimica Acta*, *71*(19), 4693–4703. https://doi.org/10.1016/j.gca.2007.07.026

Bard, E., Hamelin, B., Fairbanks, R. G., & Zindler, A. (1990). Calibration of the 14C timescale over the past 30,000 years using mass spectrometric U–Th ages from Barbados corals. *Nature*, *345*(6274), 405–410. https://doi.org/10.1038/345405a0

Bassett, S. E., Milne, G. A., Bentley, M. J., & Huybrechts, P. (2007). Modelling Antarctic sea-level data to explore the possibility of a dominant Antarctic contribution to meltwater pulse IA. *Quaternary Science Reviews*, *26*(17–18), 2113–2127. https://doi.org/10.1016/j.quascirev.2007.06.011

Bentley, M. J., Fogwill, C. J., Le Brocq, A. M., Hubbard, A. L., Sugden, D. E., Dunai, T. J., & Freeman, S. P. H. T. (2010). Deglacial history of the West Antarctic Ice Sheet in the

Weddell Sea embayment: Constraints on past Ice volume change. *Geology*, *38*(5), 411–414. https://doi.org/10.1130/G30754.1

Blanchon, P., & Shaw, J. (1995). Reef drowning during the last deglaciation-Evidence for catastrophic sea level rise and ice-sheet collapse. *Geology*, *23*(1), 4–8. https://doi.org/10.1130/0091-7613(1995)023<0004:RDDTLD>2.3.CO

Camoin, G. F., Seard, C., Deschamps, P., Webster, J. M., Abbey, E., Braga, J. C., … Dussouillez, P. (2012). Reef response to sea-level and environmental changes during the last deglaciation: Integrated ocean drilling program expedition 310, Tahiti sea level. *Geology*, *40*(7), 643–646. https://doi.org/10.1130/G32977.1

Carlson, A. E., Ullman, D. J., Anslow, F. S., He, F., Clark, P. U., Liu, Z., & Otto-Bliesner, B. L. (2012). Modeling the surface mass-balance response of the Laurentide Ice Sheet to Bølling warming and its contribution to Meltwater Pulse 1A. *Earth and Planetary Science Letters*, *315–316*, 24–29. https://doi.org/10.1016/j.epsl.2011.07.008

Cheng, H., Lawrence Edwards, R., Shen, C.-C., Polyak, V. J., Asmerom, Y., Woodhead, J., … Calvin Alexander Jr, E. (2013). Improvements in 230 Th dating, 230 Th and 234 U half-life values, and U-Th isotopic measurements by multi-collector inductively coupled plasma mass spectrometry. https://doi.org/10.1016/j.epsl.2013.04.006

Clark, P. U., Alley, R. B., Keigwin, L. D., Licciardi, J. M., Johnsen, S. J., & Wang, H. (1996). Origin of the first global meltwater pulse following the last glacial maximum. *Paleoceanography*, *11*(5), 563–577. https://doi.org/10.1029/96PA01419

Clark, P. U., Dyke, A. S., Shakum, J. D., Carlson, A. E., Clark, J., Wohlfarth, B., … McCabe, A.

M. (2009). The Last Glacial Maximum. *Science*, *325*(5941), 710–714.

Clark, P. U., Mitrovica, J. X., Milne, G. A., & Tamisiea, M. E. (2002). Sea-level fingerprint as a direct test for the source of global meltwater pulse 1{A}. *Science*, *295*(March), 2438–2441.

Deschamps, P., Durand, N., Bard, E., Hamelin, B., Camoin, G., Thomas, A. L., … Yokoyama, Y. (2012a). Ice-sheet collapse and sea-level rise at the Bølling warming 14,600 years ago. *Nature*, *483*(7391), 559–564. https://doi.org/10.1038/nature10902

Deschamps, P., Durand, N., Bard, E., Hamelin, B., Camoin, G., Thomas, A. L., … Yokoyama, Y. (2012b). Ice-sheet collapse and sea-level rise at the Bølling warming 14,600 years ago. *Nature*, *483*(7391), 559–564. https://doi.org/10.1038/nature10902

Edwards, R. L., Chen, J. H., & Wasserburg, G. J. (1987). 238 U- 234U _ 230 Th- 232 Th systematics and the precise measurement of time over the past 500 , 000 years. *Earth and Planetary Science Letters*, *81*(2–3), 175–192. https://doi.org/10.1016/0012-821X(87)90154-3

Enmar, R., Stein, M., Bar-Matthews, M., Sass, E., Katz, A., & Lazar, A. B. (n.d.). Diagenesis in live corals from the Gulf of Aqaba. I. The effect on paleo-oceanography tracers. Retrieved from https://ac-els-cdn-com.eres.library.manoa.hawaii.edu/S0016703700004178/1-s2.0-S0016703700004178-main.pdf?_tid=cebb4d77-57f8-4049-91ee-ebc2597b30c1&acdnat=1526588829_ebab8ac8e8528c7abede9bd18c9e58d7

Esat, T. M., & Yokoyama, Y. (2006). Variability in the uranium isotopic composition of the oceans over glacial-interglacial timescales. *Geochimica et Cosmochimica Acta*, *70*(16), 4140–4150. https://doi.org/10.1016/j.gca.2006.06.013

Fairbanks, R. G. (1989). A 17,000-year glacio-eustatic sea level record: influence of glacial melting rates on the Younger Dryas event and deep-ocean circulation. *Nature*, *342*(6250), 637–642. https://doi.org/10.1038/342637a0

Fleming, K., Johnston, P., Zwartz, D., Yokoyama, Y., Lambeck, K., & Chappell, J. (1998). Refining the eustatic sea-level curve since the Last Glacial Maximum using far- and intermediate-field sites. *Earth and Planetary Science Letters*, *163*(1–4), 327–342. https://doi.org/10.1016/S0012-821X(98)00198-8

Fletcher, C. H., Bochicchio, C., Conger, C. L., Engels, M. S., Feirstein, E. J., Frazer, N., … Vitousek, S. (2008). Geology of Hawaii reefs. *Coral Reefs of the U.S.A.*, 435–487. https://doi.org/10.1007/978-1-4020-6847-8_11

Golledge, N. R., Menviel, L., Carter, L., Fogwill, C. J., England, M. H., Cortese, G., & Levy, R. H. (2014). Antarctic contribution to meltwater pulse 1A from reduced Southern Ocean overturning. *Nature Communications*, *5*, 1–10. https://doi.org/10.1038/ncomms6107

Gomez, N., Gregoire, L. J., Mitrovica, J. X., & Payne, A. J. (2015). Laurentide-Cordilleran Ice Sheet saddle collapse as a contribution to meltwater pulse 1A. *Geophysical Research Letters*, *42*(10), 3954–3962. https://doi.org/10.1002/2015GL063960

Gregoire, L. J., Payne, A. J., & Valdes, P. J. (2012). Deglacial rapid sea level rises caused by ice-sheet saddle collapses. *Nature*, *487*(7406), 219–222. https://doi.org/10.1038/nature11257

Grigg, R. W. (1998). Holocene coral reef accretion in Hawaii: A function of wave exposure and sea level history. *Coral Reefs*, *17*(3), 263–272. https://doi.org/10.1007/s003380050127

Grigg, R. W., & Jones, A. T. (1997). Uplift caused by lithospheric flexure in the Hawaiian Archipelago as revealed by elevated coral deposits. *Marine Geology*, *141*(1–4), 11–25. https://doi.org/10.1016/S0025-3227(97)00069-8

Hanebuth, T., Stattegger, K., & Grootes, P. M. (2000). Rapid flooding of the Sunda Shelf: A late-glacial sea-level record. *Science*. https://doi.org/10.1126/science.288.5468.1033

Hibbert, F. D., Rohling, E. J., Dutton, A., Williams, F. H., Chutcharavan, P. M., Zhao, C., & Tamisiea, M. E. (2016a). Coral indicators of past sea-level change: A global repository of U-series dated benchmarks. *Quaternary Science Reviews*, *145*, 1–56. https://doi.org/10.1016/j.quascirev.2016.04.019

Hibbert, F. D., Rohling, E. J., Dutton, A., Williams, F. H., Chutcharavan, P. M., Zhao, C., & Tamisiea, M. E. (2016b). Coral indicators of past sea-level change: A global repository of U-series dated benchmarks. *Quaternary Science Reviews*, *145*, 1–56. https://doi.org/10.1016/J.QUASCIREV.2016.04.019

Ian G. MacIntyre, I. G. (1977). Distribution of Submarine Cements in a Modern Caribbean Fringing Reef, Galeta Point, Panama. *SEPM Journal of Sedimentary Research*, *Vol. 47*(2), 503–516. https://doi.org/10.1306/212F71C1-2B24-11D7-8648000102C1865D

Lachniet, M. S., Bernal, J. P., Asmerom, Y., & Polyak, V. (2012). Uranium loss and aragonite–calcite age discordance in a calcitized aragonite stalagmite. *Quaternary Geochronology*, *14*, 26–37. https://doi.org/10.1016/j.quageo.2012.08.003

Lambeck, K., Rouby, H., Purcell, A., Sun, Y., & Sambridge, M. (2014). Sea level and global ice volumes from the Last Glacial Maximum to the Holocene. *Proceedings of the National*

Academy of Sciences, *111*(43), 15296–15303. https://doi.org/10.1073/pnas.1411762111

Lazar, B., Enmar, R., Schossberger, M., Bar-Matthews, M., Halicz, L., & Stein, M. (2004). Diagenetic effects on the distribution of uranium in live and Holocene corals from the Gulf of Aqaba. *Geochimica et Cosmochimica Acta*, *68*(22), 4583–4593. https://doi.org/10.1016/j.gca.2004.03.029

Le Campion-Alsumard, T., Golubic, S., & Hutchings, P. (1995). Microbial endoliths in skeletons of live and dead corals: Porites lobata (Moorea, French Polynesia). *Marine Ecology Progess Series*, *117*, 149–157. Retrieved from

Liu, J., Milne, G. A., Kopp, R. E., Clark, P. U., & Shennan, I. (2016). Sea-level constraints on the amplitude and source distribution of Meltwater Pulse 1A. *Nature Geoscience*, *9*(2), 130–134. https://doi.org/10.1038/ngeo2616

Muhs, D. ., & Szabo, B. . (1994). New uranium-series ages of the Waimanalo Limestone, Oahu, Hawaii: Implications for sea level during the last interglacial period. *Marine Geology*, *118*(3–4), 315–326. https://doi.org/10.1016/0025-3227(94)90091-4

Muhs, D. R., Wehmiller, J. F., Simmons, K. R., & York, L. L. (2003). Quaternary sea-level history of the United States. *Developments in Quaternary Science*, *1*(C), 147–183. https://doi.org/10.1016/S1571-0866(03)01008-X

Peltier, W. R. (2002). On eustatic sea level history: Last Glacial Maximum to Holocene. *Quaternary Science Reviews*, *21*(1–3), 377–396. https://doi.org/10.1016/S0277-3791(01)00084-1

Peltier, W. R. (2005). On the hemispheric origins of meltwater pulse 1a. *Quaternary Science Reviews*, *24*(14–15), 1655–1671. https://doi.org/10.1016/j.quascirev.2004.06.023

Ribaud-Laurenti, A., Hamelin, B., Montaggioni, L., & Cardinal, D. (2001). Diagenesis and its impact on Sr/Ca ratio in Holocene Acropora corals. *International Journal of Earth Sciences*, *90*(2), 438–451. https://doi.org/10.1007/s005310000168

Rubin, K. H., Fletcher, C. H., & Sherman, C. (2000). Fossiliferous Lana'i deposits formed by multiple events rather than a single giant tsunami. *Nature*, *408*(6813), 675–681. https://doi.org/10.1038/35047008

Sanborn, K. L., Webster, J. M., Yokoyama, Y., Dutton, A., Braga, J. C., Clague, D. A., … Hansen, J. R. (2017). New evidence of Hawaiian coral reef drowning in response to meltwater pulse-1A. *Quaternary Science Reviews*, *175*, 60–72. https://doi.org/10.1016/j.quascirev.2017.08.022

Sayani, H. R., Cobb, K. M., Cohen, A. L., Elliott, W. C., Nurhati, I. S., Dunbar, R. B., … Zaunbrecher, L. K. (n.d.). Effects of diagenesis on paleoclimate reconstructions from modern and young fossil corals. https://doi.org/10.1016/j.gca.2011.08.026

Scholz, D., & Mangini, A. (2007). How precise are U-series coral ages? *Geochimica et Cosmochimica Acta*, *71*(8), 1935–1948. https://doi.org/10.1016/j.gca.2007.01.016

Sherman, C. E., Fletcher, C. H., & Rubin, K. H. (1999). MARINE AND METEORIC DIAGENESIS OF PLEISTOCENE CARBONATES FROM A NEARSHORE SUBMARINE TERRACE, OAHU, HAWAII, *69*(5), 1083–1097. Retrieved from http://www.soest.hawaii.edu/coasts/publications/sherman_JSR_1999.pdf

Stanford, J. D., Rohling, E. J., Hunter, S. E., Roberts, A. P., Rasmussen, S. O., Bard, E., … Fairbanks, R. G. (2006). Timing of meltwater pulse 1a and climate responses to meltwater injections. *Paleoceanography*, *21*(4), 1–9. https://doi.org/10.1029/2006PA001340

Tarasov, L., & Peltier, W. R. (2006). A calibrated deglacial drainage chronology for the North American continent: evidence of an Arctic trigger for the Younger Dryas. *Quaternary Science Reviews*, *25*(7–8), 659–688. https://doi.org/10.1016/j.quascirev.2005.12.006

Thompson, W. G., Spiegelman, M. W., Goldstein, S. L., & Speed, R. C. (2003). An open-system model for U-series age determinations of fossil corals. *Earth and Planetary Science Letters*, *210*(1–2), 365–381. https://doi.org/10.1016/S0012-821X(03)00121-3

Tribollet, A. (2008). The boring microflora in modern coral reef ecosystems: A review of its roles Bioerosion in changing environments View project Developement of French tropical Islands and impacts of climate change on coral reefs View project. https://doi.org/10.1007/978-3-540-77598-0_4

Watts, A. B., & ten Brink, U. S. (1989). Crustal structure, flexure, and subsidence history of the Hawaiian Islands. *Journal of Geophysical Research: Solid Earth*, *94*(B8), 10473–10500. https://doi.org/10.1029/JB094iB08p10473

Webster, J. M., Braga, J. C., Humblet, M., Potts, D. C., Iryu, Y., Yokoyama, Y., … Lougheed, B. C. (2018). Response of the Great Barrier Reef to sea-level and environmental changes over the past 30,000 years. *Nature Geoscience*, *11*(6), 426–432. https://doi.org/10.1038/s41561-018-0127-3

Webster, J. M., Clague, D. A., Braga, J. C., Spalding, H., Renema, W., Kelley, C., … Potts, D.

(2006). Drowned coralline algal dominated deposits off Lanai, Hawaii; carbonate accretion and vertical tectonics over the last 30 ka. *Marine Geology*, *225*(1–4), 223–246. https://doi.org/10.1016/J.MARGEO.2005.08.002

Webster, J. M., Clague, D. A., Riker-Coleman, K., Gallup, C., Braga, J. C., Potts, D., … Paull, C. K. (2004). Drowning of the - 150 m reef off Hawaii: A casualty of global meltwater pulse 1A? *Geology*, *32*(3), 249–252. https://doi.org/10.1130/G20170.1